A REDEFINED HYDRAULIC DIAMETER FOR LAMINAR FLOW(U) AIR FORCE INST OF TECH WRIGHT-PATTERSON AFB OH SCHOOL OF ENGINEERING   B J SUTHERLAND 01 DEC 86

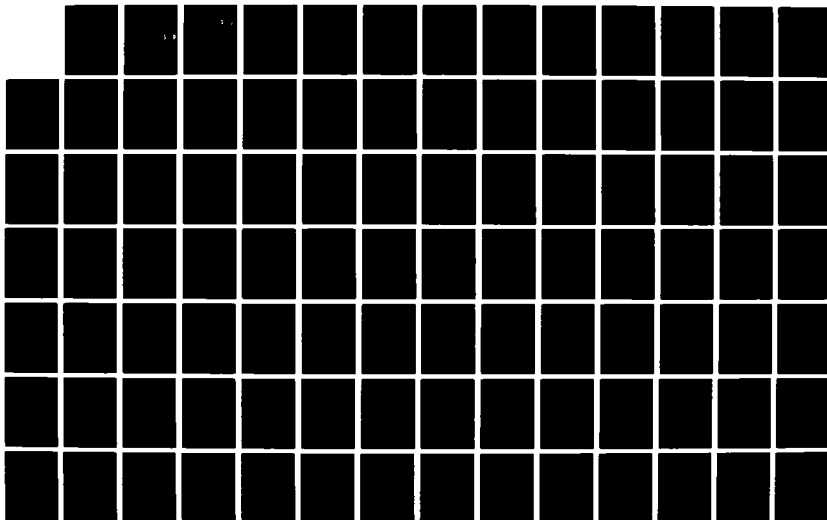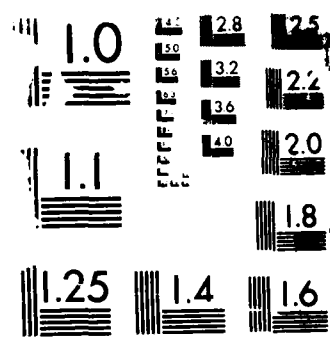UNCLASSIFIED   AFIT/GAE/AA/86D-17

F/G 20/4   NL

AD-A179 511

A REDEFINED HYDRAULIC DIAMETER

FOR LAMINAR FLOW

THESIS

Bruce J. Sutherland
Captain, USAF

AFIT/GAE/AA/86D-17

DEPARTMENT OF THE AIR FORCE

AIR UNIVERSITY

AIR FORCE INSTITUTE OF TECHNOLOGY

Wright-Patterson Air Force Base, Ohio

87 4 16 030

DTIC
SELECTED
APR 1 6 1987
S
D

A REDEFINED HYDRAULIC DIAMETER

FOR LAMINAR FLOW

THESIS

Bruce J. Sutherland
Captain, USAF

AFIT/GAE/AA/86D-17

Approved for public release; distribution unlimited

A REDEFINED HYDRAULIC DIAMETER

FOR LAMINAR FLOW

THESIS

Presented to the Faculty of the School of Engineering

of the Air Force Institute of Technology

Air University

In Partial Fulfillment of the

Requirements for the Degree of

Master of Science in Aeronautical Engineering

Bruce J. Sutherland, B.S.

Captain, USAF

December 1986

Accesion For		
NTIS CRA&I		☑
DTIC TAB		[]
Unannounced		[]
Justification		
By		
Distribution /		
Availability Codes		
Dist	Avail and/or Special	
A-1		

Acknowledgements

The experimental portion of this investigation was performed at facilities of the Air Force Institute of Technology, Wright-Patterson AFB, Ohio.

In performing this investigation I have had a great deal of help from others. I am deeply indebted to my faculty advisor, Dr. James Hitchcock, whose continuing patience and guidance were essential for the completion of this study. In addition, I would like to thank my committee members, Dr. William Elrod and Dr. Milton Franke, for their enthusiasm and support of this investigation.

I would also like to thank Leroy Cannon, Jay Anderson, and Nick Yardich for their fantastic support in operating and maintaining the experimental apparatus. Also a word of thanks is owed to the people of the Model Fabrication Shop, in particular, Joe Hofele, for their excellent job of preparing the materials used in this experiment.

I extend my deepest appreciation to my wife Patricia and daughter Lauren for their unwavering support and encouragement during this ordeal.

Computer used: ATARI 130XE

Software: PAPERCLIP by Batteries Included

Printer: PANASONIC KX-P1091

Bruce J. Sutherland

Table of Contents

List of Figures

vi

List of Tables

List of Symbols

A	Duct cross-sectional area
AE	Area of Duct - area of modelling circle
As	Duct surface area
C_f	Fanning friction factor
D_h	Hydraulic diameter
$D_{h,1}$	New hydraulic diameter
D_m	Modelling circle diameter
L^*	Hydrodynamic entrance length, non-dim. form
$\dot{m}$	Mass flow rate
P	Static pressure
PE	Perimeter of duct + perimeter of modelling circle
Per	Duct perimeter
Re	Reynolds number
Re_{tr}	Transition Reynolds number
V	Average duct velocity
X	Hydrodynamic entrance length
α	Aspect ratio
δ	Boundary layer thickness
λ	Darcy friction factor
μ	Dynamic viscosity
ν	Kinematic viscosity
ρ	Fluid density
τ_0	Shear stress at the duct wall

x

Abstract

For laminar, steady flow in ducts, the current definition of hydraulic diameter, D_h, does not accurately depict the non-uniform wall shear stress distribution around the perimeter of non-circular duct shapes. In this investigation, a new hydraulic diameter, $D_{h,i}$, was empirically determined. It correlated friction factor data for many non-circular shapes to within approximately 2.4 % of the circular duct value.

An experiment, using the AFIT Oil Flow Rig Set-up, was run to determine the effect on transition Reynolds number, Re_{tr}, and hydrodynamic entrance length, L^+, of replacing D_h with $D_{h,i}$. Transition Reynolds number and L^+ were determined, based on D_h and $D_{h,i}$, for a circular, square, and concentric annular duct.

Transition Reynolds numbers, based on D_h, for the square and concentric annular ducts were approximately 12.5 % lower than the circular duct Re_{tr}. The Re_{tr}, based on $D_{h,i}$, did not correlate well for the concentric annulus, but did correlate for the square duct.

Hydrodynamic entrance lengths, based on D_h and $D_{h,i}$, were experimentally determined for the circular and square duct only. The square duct L^+, and the analytic concentric annular duct L^+, based on $D_{h,i}$, did not correlate to the

to the circular duct value.

Although the Re_{ψ} and L^* for the square and concentric annular ducts did not correlate well when based on $D_{h,i}$, the data obtained is still useful to the engineering community since it provides an addition data base for experimental L^*, and provides experimental data on Re_{ψ} for square and concentric annular ducts.

A REDEFINED HYDRAULIC DIAMETER FOR LAMINAR FLOW

I.   Introduction

Background

For flow in circular ducts, where there is a uniform
wall shear stress around the perimeter and uniform distance
from the center to the surface, duct radius, or diameter,
is a logical choice for the characteristic dimension in
flow correlations. For non-circular ducts a characteristic
dimension, the hydraulic diameter (D_h), has been defined as
4A/P where A is the duct cross-sectional area and P is
the duct perimeter. The hydraulic diameter is
unambiguously defined for any cross-sectional shape, and
for consistency is used in both turbulent and laminar duct
flows. Experimentation has verified that, for turbulent
flow, where the wall shearing stress is fairly uniform
around the perimeter, the hydraulic diameter is the
appropriate characteristic dimension for many non-circular
duct shapes (1). For fully developed, laminar flow,
however, the wall shearing stress distribution along the
perimeter of non-circular ducts is not uniform and the
hydraulic diameter is, perhaps, not the best characteristic
dimension. For example, for a circular duct, $C_f Re$ = 16.0,
while for a triangular duct, $C_f Re$ = 13.333, where Re is

1

defined as VD_h/ν. At present there is no characteristic

dimension that correlates laminar flow data in non-circular

ducts.

Some current uses of hydraulic diameter as a

characteristic dimension are in transition Reynolds number

and hydrodynamic entrance length calculations. Reynolds

number, which is a ratio of inertia to viscous forces, is

very much associated with the stability of laminar flows.

Viscous forces tend to restore laminar flow after a

disturbance, while inertia forces tend to amplify

disturbances, therefore, transition from laminar to

turbulent flow might be characterized by a transition

Reynolds number, Re_{tr}. For circular duct flow, the Re_{tr},

based on diameter and duct averaged velocity, is

approxiamately 2000 (2). This author has not found any

Re_{tr} data for non-circular ducts, and since the wall

shearing stress is not uniformly distributed around the

perimeter of non-circular ducts, one would speculate that

the Re_{tr}, based on hydraulic diameter, for these ducts

would be different from the circular duct value of 2000.

Another use of hydraulic diameter has been in

hydrodynamic entrance length (X) calculations. One of the

most common definitions of X is the duct length required to

achieve a duct centerline velocity 99% of the fully

developed value (3). These results are often given in the

non-dimensional form, $L^* = (X/D_h)/Re$. Several different

2

analytical solutions to the L* problem exist for circular as well as non-circular duct shapes (14). Based on hydraulic diameter, L* varies significantly for each duct shape. Little, if any, experimental L* data has been reported.

Objectives

This investigation had four objectives:

1. Empirically determine a new hydraulic diameter, "$D_{h,1}$", that better represents the mean center to surface distance for laminar flow in non-circular ducts, and which correlates C_fRe data.

2. Experimentally determine the Re_{tr}, based on $D_{h,1}$, for a circular duct, square duct, and concentric annulus with an aspect ratio that simulates flow between infinite parallel plates.

3. Experimentally determine L* for the above shapes, based on $D_{h,1}$.

4. Examine the effect on Re_{tr} and L* of replacing the traditional D_h with $D_{h,1}$

The first objective will be accomplished using friction factors (C_fRe), for fully developed duct flow, as the data base for the $D_{h,1}$ calculations, with an attempt to converge the data to the circular duct value.

The remaining objectives will be accomplished using

3

the Air Force Institute of Technology's instrumented oil
flow rig set-up. Pressure and mass flow data will be taken
for the different duct shapes to determine Re_{cr} and L^*.

II. <u>Duct Theory</u>

<u>Circular Ducts</u>

The circular duct is the most common duct shape in use today. For constant-property, steady, fully-developed, laminar flow through circular ducts, as in Figure 1, the equation of motion can be written as:

$$(\mu/r)[(\partial/\partial r)(r(\partial u/\partial r))] = dP/dx \qquad (1)$$

Since the pressure is independent of r, Equation (1) can be integrated directly with respect to r to obtain the velocity profile. Applying boundary conditions:

At	$r = 0$	axis of the tube
	$\partial u/\partial r = 0$	velocity gradient is zero
At	$r = r_0$	duct wall
	$u = 0$	no slip at the wall

yields

$$u = (r_0^2/4\mu)(-dP/dx)(1-(r^2/r_0^2)) \qquad (2)$$

It proves more convienient to express this velocity in terms of a mean duct velocity, V, rather than the pressure gradient. For incompressible flow, the mean velocity is defined as:

$$V = (\iint u dA)/A$$

resulting in,

$$V = (r_0^2/8\mu)(-dP/dx) \qquad (3)$$

thus,

$$u = 2V(1-(r/r_0)^2) \qquad (4)$$

5
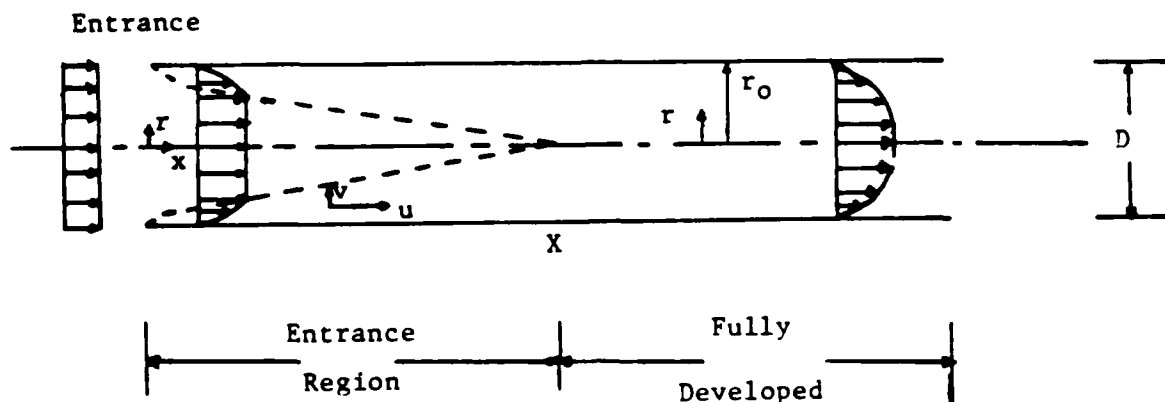
Figure 1. Flow in a Circular Duct

The gradient of this velocity profile is used to evaluate the shear stress at the wall.

$$\tau_0 = \mu \, (\partial u / \partial r)_{r=r_0} \qquad (5)$$

Using Equation (4)

$$\tau_0 = \mu \, [2V(-2r/r_0{}^2)]_{r_0} = -4V\mu/r_0 \qquad (6)$$

Since V is constant for steady, fully-developed flow, τ_0 is constant. The friction factor can now be evaluated. The Fanning friction factor (C_f) is defined as the ratio of wall shearing stress to the dynamic head of the flow.

$$C_f = \tau_0 / (\rho V^2 / 2) \qquad (7)$$

thus,

$$C_f = (4V\mu/r_0)/(\rho V^2/2) = 8\mu/\rho V r_0 \qquad (8)$$

6

For a circular duct, Re is defined as

$$Re = \rho VD/\mu$$

where $D = 2r_o$. Rewriting Equation (8)

$$C_f = 16/Re \qquad (9)$$

Data from Stanton and Pannell (6:199) and Senecal and
Rothfus (7:533) verifies this equation up to a Re of 2000.

Non-Circular Ducts.

Although a majority of ducts in use today are of
circular cross-section, many non-circular duct applications
exist and require further flow analysis. For constant
property, fully developed, laminar flow through a
non-circular duct, the equation of motion is:

$$\partial^2 u/\partial y^2 + \partial^2 u/\partial z^2 = (1/\mu)(\partial P/\partial x)$$

The friction forces are seen to be functions of the
cross-sectional dimensions in both y and z directions.
Traditionally, a single length dimension, the hydraulic
diameter (D_h), has been used to characterize the
cross-section. Hydraulic diameter is related to the
hydraulic radius, R_h, which is the ratio of cross-sectional
area, A, to wetted perimeter, Per, by:

$$D_h = 4R_h = 4A/Per$$

Hydraulic diameter for a non-circular duct is intended to
represent the diameter of an equivalent circular duct which
has the same C_fRe as the non-circular duct. Table I
illustrates D_h for several non-circular shapes.

7

TABLE I.

Five Ducts With the Same Hydraulic Diameter   (5:77)

Cross section

Circular $D_h = s$

Square $D_h = s$ D_h

Equilateral triangle $D_h = s/\sqrt{3}$ D_h

Rectangular (4 1) $D_h = 8s/5$

Infinite parallel plates $D_h = 2s$
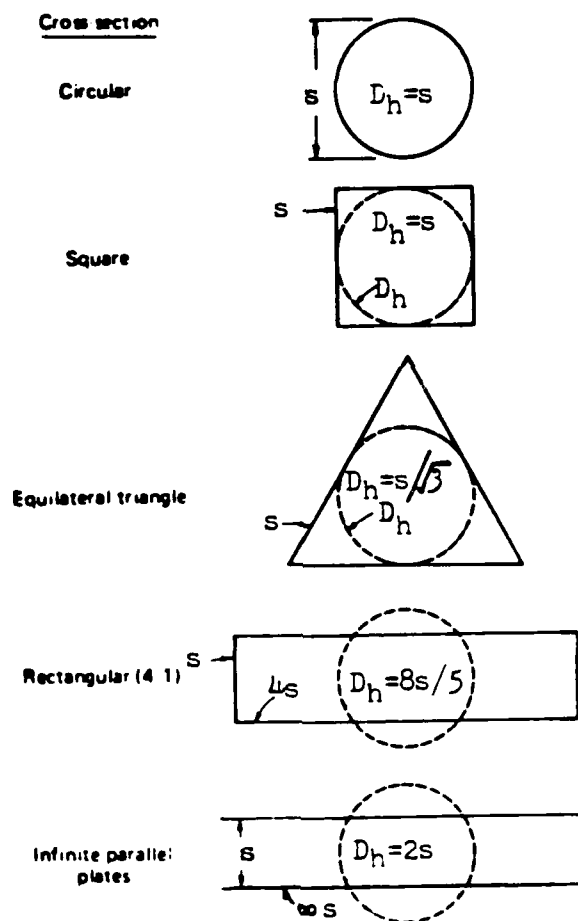
Turbulent flow through non-circular ducts, using D_h as the characteristic dimension, was investigated by Shiller (8) and Nikuradse (9), who verified that D_h provided satisfactory results. For laminar flows, however, the Shiller and Nikuradse data, as well as that of Koch and Feind (10), showed limitations to the use of hydraulic diameter. This data is shown in Figure 2 from Schlicting (2:576). Here λ is the Blasius, or Darcy, friction factor where,

$$\lambda = 64/Re = 4C_f$$

for circular ducts. In Figure 2, λ has been multiplied by a constant, for each duct shape, in order to fit all the data onto one graph. For laminar flow, the hashed lines represent a circular duct. Note the difference in λ between circular and non-circular ducts based on D_h.
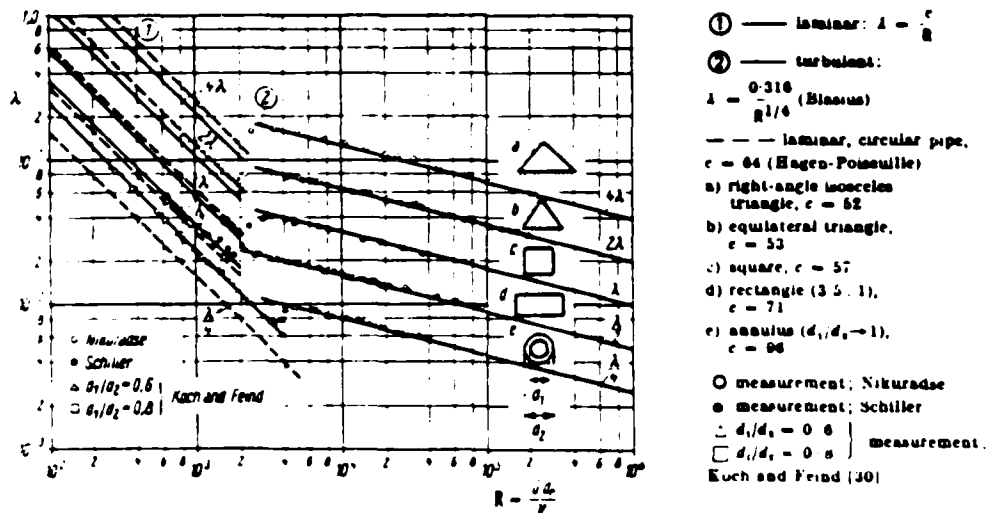
Figure 2. Friction Factor for Several Ducts

Exact solutions to the equations of motion, for many

non-circular ducts, based on D_h, yield,

$$C_fRe = C = \text{constant}$$

for each duct shape, instead of the desired circular duct

solution, $C_fRe = 16$. Several values of C_fRe are shown in

Table II (11).

TABLE II.

C_fRe for Non-Circular Ducts

DUCT SHAPE	$C = C_fRe$
SINE	12.630
TRIANGLE	13.333
SQUARE	14.227
HEXAGON	15.054
RECTANGLE 2:1	15.548
SEMI-CIRCLE	15.600
RECTANGLE 4:1	18.233
RECTANGLE 8:1	20.585
INFINITE PARALLEL PLATES	24.000

These values of C_fRe represent exact solutions, based on

D_h, most having been verified by experimental data

(8,9,10).

By examining the definition of hydraulic radius, an

insight as to why these laminar flow values do not correlate with the equivalent circular duct data can be gained. The reciprocal of hydraulic radius is the wetted perimeter per unit of flow cross-section and describes the amount of wall area in contact with the moving fluid. The hydraulic radius is a good index if the resistance to momentum transfer is predominantly dependent on the amount of wall surface area, as it is in turbulent flow. In laminar flows this resistance to momentum transfer takes place throughout the cross-sectional flow area and is not primarily associated with the wall surfaces. Thus reliable conversions from circular to non-circular shapes cannot be expected.

Another explanation for poor correlation with laminar flows is seen by examining the surface area per unit of flow volume, As/Vol, for individual ducts. The friction factor is directly related to the amount of wall shear stress and this stress is related to the amount of surface area it acts upon. For ducts with As/Vol different than that of a circular duct, the shearing stress is acting on a different amount of surface area, per unit volume, and a different C_f can be expected. For example, a rectangular duct with an aspect ratio of 8:1, has more surface area, per unit volume, for the shearing stress to act upon than does the circular duct with the same D_h, and hence a larger C_f is expected.

11

Flow in the corners of non-circular ducts also influences C_f. Consider a square duct and a circular duct, each with the same D_h. Each duct has approximately the same As/Vol ratio. In the corners of the square duct, the velocity is low compared to V, and with this low velocity is low shearing stress. This low velocity, in essence, reduces the _effective_ flow area. Low effective flow area produces a lower C_f for the square duct compared to the circular duct.

Since laminar flow C_fRe values do not correlate well for non-circular ducts, it becomes desirable to have exact solutions for non-circular shapes, based on a new $D_{h,1}$, where the value of C_fRe for these ducts equals that of the circular duct. Individual C_fRe, as in Table II, would no longer be necessary.

Exact C_fRe values vary non-linearly for rectangular ducts, from the square duct value of 14.227, to the infinite parallel plate duct value of 24.0, as illustrated in Figure 3 (1). Since the corners of rectangular ducts have the same influence on C_f, from duct to duct, the C_fRe variance can be directly attributed to the difference in As/Vol. Once again, the values in Figure 3 are based on D_h. As noted in Figure 3, a rectangular duct with an aspect ratio of approximately 2.3 has a C_fRe equal to that of a circular duct, and D_h becomes an appropriate dimension.

12
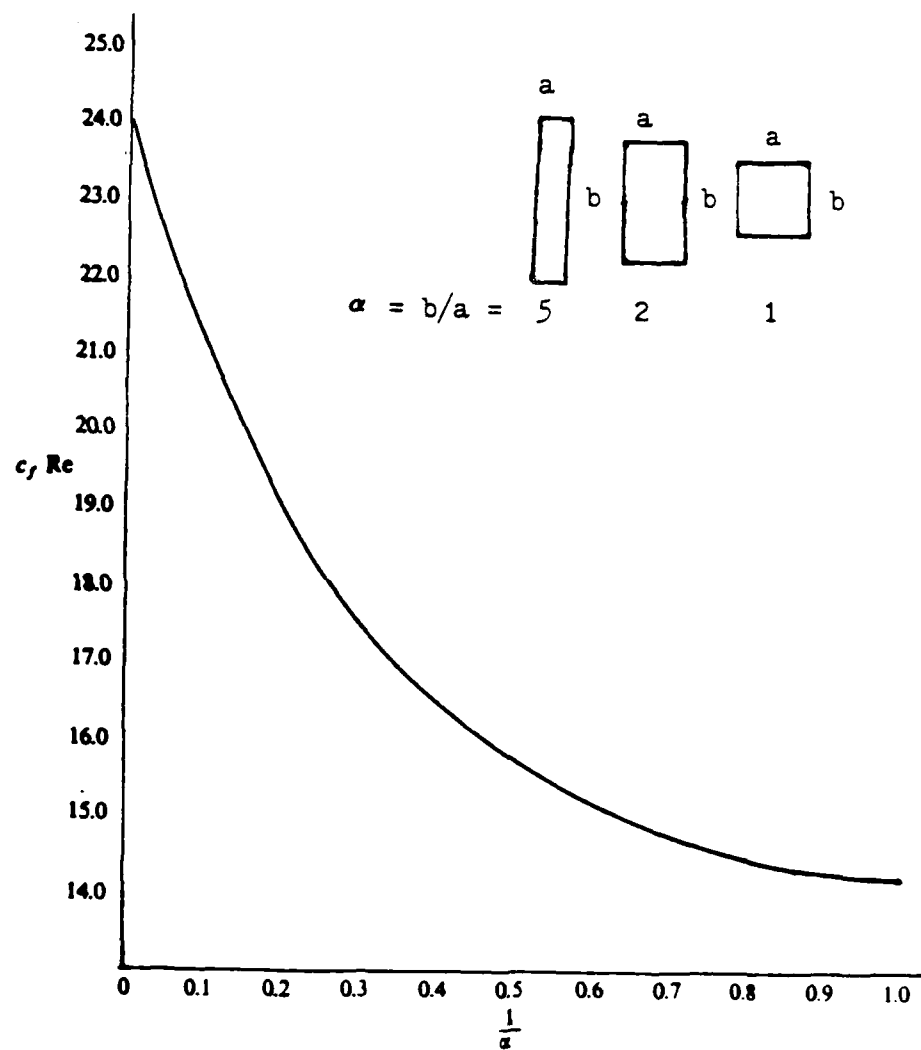
Figure 3. Friction Coefficients for Rectangular Ducts

III.   Redefined Hydraulic Diameter

Approach

Currently, each non-circular duct has a unique exact solution for $C_f Re$, based on D_h. This author seeks a new parameter, $D_{h,1}$, that would produce a non-circular duct value of $C_f Re$ equal to the circular duct value of 16. The first step is to examine the $C_f Re$ data for several non-circular duct shapes, where

$$Re = \rho V D_h / \mu$$

Table II and Figure 3 summarize $C_f Re$, based on D_h, for many of the most common non-circular shapes. An empirical equation for $D_{h,1}$ will be derived that will correlate $C_f Re$ data to the circular duct. To do this, first the data from square, triangular, hexagonal, and semi-circular ducts are examined, since these shapes are similiar, in that they are fairly compact. Next the rectangular data from Figure 3 is approximated, to within 0.05%, by the following equation:

$$C_f Re = 24[1 - (1.3553/\alpha) + (1.9467/\alpha^2) - (1.7012/\alpha^3)$$
$$+ (.9564/\alpha^4) - (.2537/\alpha^5)] \qquad (3:199)$$

The rectangular duct will be examined first for α from 1.0 to 10., in increments of 0.25. Most manufactured rectangular ducts are in this range, so small increments are taken to fully evaluate these ducts. Aspect ratios of 25, 50, 100, and ∞ were examined next. These ducts

14

represent flow that is beginning to simulate infinite parallel plate flow.

The hydraulic diameter describes the diameter of an equivalent circular duct which has the same mean shear stress as the non-circular duct. Since D_h under-estimates the correct diameter in some cases, such as square and triangular ducts, and over-estimates it in others, such as infinite parallel plates and elongated rectangular ducts, a new D_h, $D_{h,1}$, is invisioned. $D_{h,1}$ is determined using a "modelling circle" diameter, D_m, plus a correction factor. This "modelling circle" represents the area of "main flow" in the duct. It, in essence, separates the corner areas from the "main area" in the duct. Table III illustrates the modelling circles for several duct shapes. For fairly compact shapes, such as square, triangular, and hexagonal ducts, the modelling circle area is identically the D_h area, and $D_m = D_h$. For elongated ducts, such as infinite parallel plates or rectangular ducts, where the flow extends out, the modelling cirle is an ellipse where the elliptic aspect ratio is the same as that of the duct. For simplicity, D_m is the smaller length, a, for elliptical modelling circles. Comparing the flow area of circles with diameter D_h and their associated perimeter to those of the elliptical modelling circles, shows that the elliptical modelling circles better represents the actual flow area, and the perimeter upon which the mean shear stress may act.

15

TABLE III.

Modelling Circles for Several Duct Shapes

D_a	= 1.000 S
D_b	= 1.000 S

D_m, S

D_a	= .57735 S
D_b	= .57735 S

S

D_a	= 1.732 S
D_b	= 1.732 S

S

$2b/2a = 1.3$

D_a	= .500 S
D_b	= .611 S

S

$2b/2a = 2$ a b S

D_a	= 1.000 S
D_b	= 1.333 S

$2b/2a = 4$ D_m S

D_a	= 1.000 S
D_b	= 1.600 S

$2b/2a = \infty$ S

D_a	= 1.000 S
D_b	= 2.000 S

16

This can be seen, for example, for the rectangular duct of α = 4:1, by comparing the sketches in Table I and Table III. In determining a correction factor for $D_\bullet$, the area between the duct walls and the modelling circle, and its associated perimeter, is utilized.

Results

For laminar flow in non-circular ducts:

$$D_{h,1} = 3.2(AE/PE)(D_h/D_\bullet) + D_\bullet \qquad (10)$$

where

AE = area of the duct - area of the "modelling circle"

PE = perimeter of the duct + perimeter of the "modelling circle"

D_h = hydraulic diameter, 4A/P

$D_\bullet$ = smallest diameter of elliptic "modelling circle"

Figure 4 shows an example of AE and its associated perimeter. Equation (10) is used for all ducts except rectangular ones. An additional term is needed for rectangular ducts to account for the changing $D_h/D_\bullet$ ratio and the aspect ratio, α. For rectangular ducts:

$$D_{h,1} = 3.2(AE/PE)(D_h/D_\bullet)[1 + [4(D_h - D_\bullet)^{\cdot 5}/\alpha]] + D_\bullet \quad (11)$$

For example, using Figure 4 and Equation (11),

area of the duct = $3S^2$

area of the "modelling circle" = $\pi(.5S)(1.5S)$

perimeter of the duct = 8S

perimeter of "modelling circle" = $2\pi[(1.5^2 + .5^2)/2]^{\cdot 5}S$

17
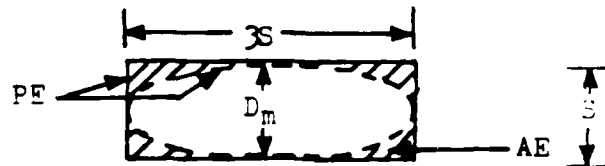
Figure 4.   AE for a Rectangular Duct

$AE = .644S^2$

$PE = 15.02S$

aspect ratio = 3.0

$D_h = 1.5S$

$D_e = 1.0S$

and,

$D_{h,i} = 1.4S$

Here, for an ellipse:

$$Area = \pi ab$$

and the perimeter can be approximated by,

$$Perimeter \quad 2\pi[(a^2 + b^2)/2]^{.5}$$

Note that equation (11) reduces to equation (10) for the limiting cases of the square duct ($D_h = D_e$) and the infinite parallel plate duct ($\alpha = \infty$).

Table IV and V present $D_{h,i}$ and C_fRe data, based on $D_{h,i}$. Friction factors for all duct shapes investigated, are within 2.4% of the circular duct value of 16.0. Appendix A presents a breakdown of the $D_{h,i}$ calculations for each duct shape.

18

TABLE IV.

Redefined Hydraulic Diameter, $D_{h,1}$

SHAPE	$C_f Re\,(D_h)$	D_h	D_m	$D_{h,1}$	$C_f Re\,(D_{h,1})$	$\Delta\%$
SQUARE	14.227	1.000S	1.000S	1.098S	15.62	-2.40
TRIANGLE	13.333	0.577S	0.577S	0.693S	15.94	-0.04
HEXAGON	15.054	1.732S	1.732S	1.800S	15.64	-2.20
SEMI-CIR	15.600	0.611S	0.500S	0.633S	16.15	0.94
INF.PAR.PL.	24.000	2.000S	1.000S	1.345S	16.12	0.75

TABLE V.

Redefined Hydraulic Diameter, $D_{h,i}$

Rectangular Ducts

Aspect Ratio	$C_f Re\,(D_h)$	D_h	$D_{h,i}$	$C_f Re\,(D_{h,i})$	Δ %
1.00	14.230	1.000S	1.098S	15.620	− 2.4
1.25	14.382	1.111S	1.239S	16.039	0.2
1.50	14.715	1.200S	1.294S	15.863	− 0.9
1.75	15.127	1.273S	1.328S	15.786	− 1.3
2.00	15.557	1.333S	1.352S	15.770	− 1.4
2.25	15.978	1.385S	1.368S	15.783	− 1.4
2.50	16.377	1.429S	1.379S	15.810	− 1.2
2.75	16.749	1.467S	1.387S	15.843	− 1.0
3.00	17.095	1.500S	1.393S	15.877	− 0.8
3.25	17.414	1.529S	1.397S	15.909	− 0.6
3.50	17.710	1.556S	1.400S	15.940	− 0.4
3.75	17.982	1.579S	1.402S	15.969	− 0.2
4.00	18.234	1.600S	1.404S	15.995	− 0.0
4.25	18.467	1.619S	1.404S	16.019	0.1
4.50	18.684	1.636S	1.405S	16.040	0.3
4.75	18.885	1.652S	1.405S	16.060	0.4
5.00	19.072	1.667S	1.405S	16.078	0.5
5.25	19.246	1.680S	1.405S	16.095	0.6
5.50	19.409	1.692S	1.405S	16.110	0.7
5.75	19.561	1.704S	1.404S	16.124	0.8
6.00	19.705	1.714S	1.404S	16.136	0.9
6.25	19.839	1.724S	1.403S	16.148	0.9
6.50	19.965	1.733S	1.403S	16.159	1.0
6.75	20.084	1.742S	1.402S	16.170	1.1
7.00	20.197	1.750S	1.402S	16.180	1.1
7.25	20.303	1.758S	1.401S	16.189	1.2
7.50	20.404	1.765S	1.401S	16.197	1.2
7.75	20.499	1.771S	1.400S	16.206	1.3
8.00	20.590	1.778S	1.400S	16.214	1.3
8.25	20.676	1.784S	1.399S	16.221	1.4
8.50	20.758	1.789S	1.399S	16.229	1.4
8.75	20.836	1.795S	1.399S	16.236	1.5
9.00	20.910	1.800S	1.398S	16.242	1.5
9.25	20.981	1.805S	1.398S	16.249	1.6
9.50	21.049	1.810S	1.397S	16.255	1.6
9.75	21.114	1.814S	1.397S	16.262	1.6
10.00	21.176	1.818S	1.397S	16.268	1.7
25.00	22.770	1.923S	1.370S	16.218	1.4
50.00	23.370	1.961S	1.358S	16.178	1.1
100.00	23.680	1.980S	1.351S	16.154	1.0
∞	24.000	2.000S	1.343S	16.120	0.8

IV. <u>Experimentation</u>

<u>Apparatus</u>

The AFIT Oil Flow Rig Set-Up, shown in Figure 5, was used to determine Re_{ur}, L^{*}, and C_r for a circular, square, and concentric annular duct. Oil is pumped from the reservoir, up to the duct entrance, down the duct, and either into a weighing tank or back into the reservoir, depending on the selector valve setting. A mercury manometer board displays individual pressures for 10 static pressure stations along the duct.

SAE 10W-10 oil is the working fluid for this experiment. To determine Re_{ur}, L^{*}, and C_r, the density (ρ) and the viscosity (μ) of the oil are needed. The density of the oil is determined by,

$$\rho_{oil} = \rho_{H2O}(\text{specific gravity of oil})$$

The density of water is 62.4 lbm/ft³, and the specific gravity of oil is the ratio of the mass of a given volume of oil to that of an equal volume of water. Six measurements were taken with an average specific gravity, for this oil, of .863 (see Appendix B.). Thus, the density of the oil is 53.85 lbm/ft³.

The viscosity of the oil can be determined by using the Hagen-Poiseuille law (20:114), or by use of a viscometer. Lieutenant J. C. Ghiglieri (29), determined ν to be:

21

Scale

Weighing
Tank

Selector Valve

Manometer
Board

10

9

8

7

6

5

4

3

2

1

Static Pressure Taps

Oil Reservoir

Mass Flow Valve

Pump
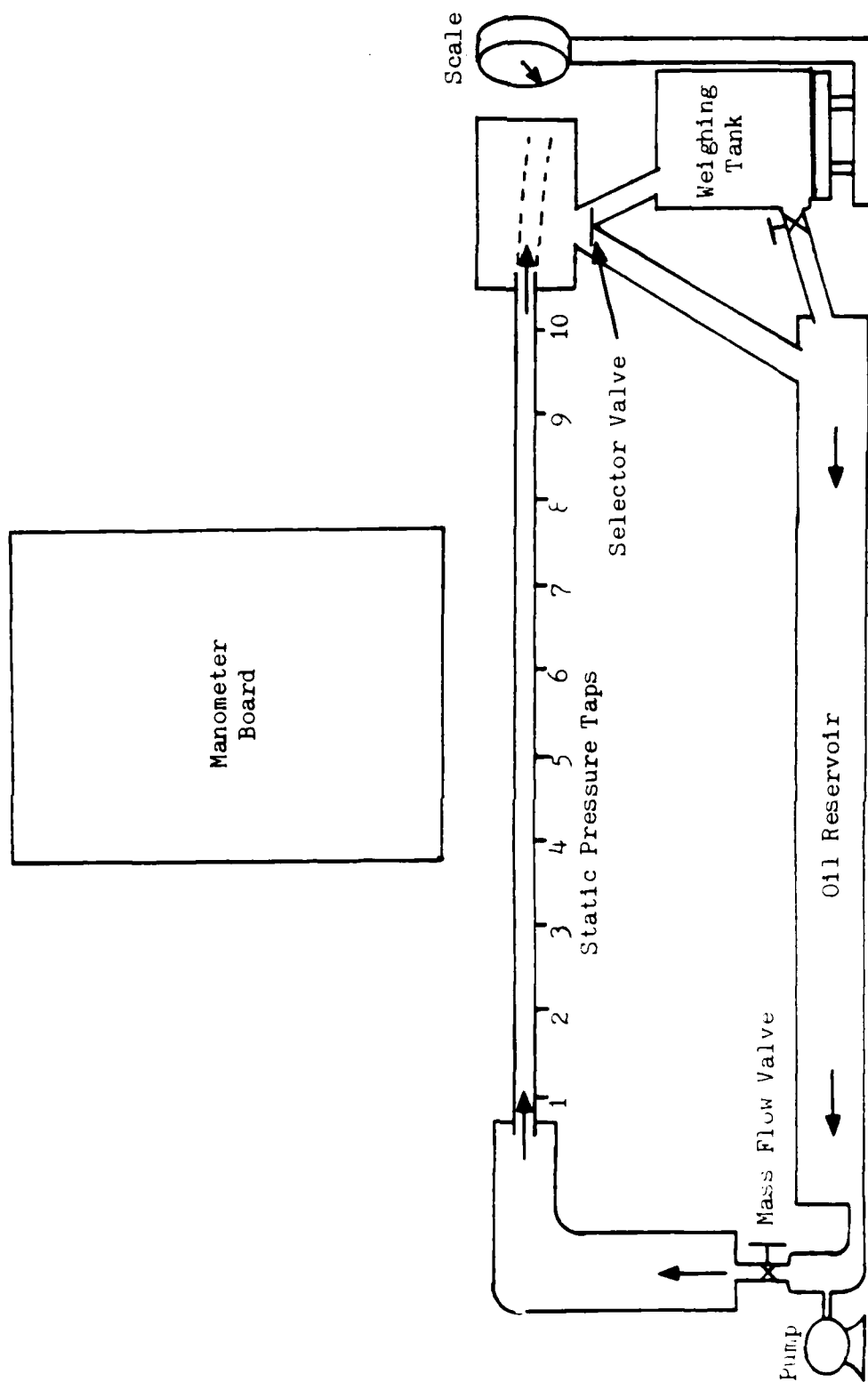
Figure 5. Oil Flow Rig Set-up

22

$$100 \text{ F} \quad - \quad 10.18 \text{ centistokes}$$

$$210 \text{ F} \quad - \quad 2.53 \text{ centistokes}$$

Using a Viscosity-Temperature chart, like that shown in Figure 6, these values can be linearized and μ at other temperatures extrapolated. Table VI shows some extrapolated values. These values were verified from the circular duct data using the Hagen-Poiseuille law,

$$dP/dx = (128 \mu Q)/(\pi D^4)$$

where,

$$Q = \dot{m}/\rho = AV$$

Circular Duct

Figure 7 shows a diagram of the circular duct that was used for this experiment. The duct is 21 feet long, with an inside diameter of 0.8125 inches. Ten static pressure taps are mounted along the duct with the first tap 8 inches from the entrance, and the remaining 9 taps located every 2 feet downstream. The cross-sectional flow area is 0.5185 square inches.

Square Duct

The square duct, shown in Figure 8, is 21 feet long, with an inside width of 0.75 inches. Pressure taps are mounted identical to those of the circular duct. The cross-sectional flow area for this duct is 0.5625 square inches.

23
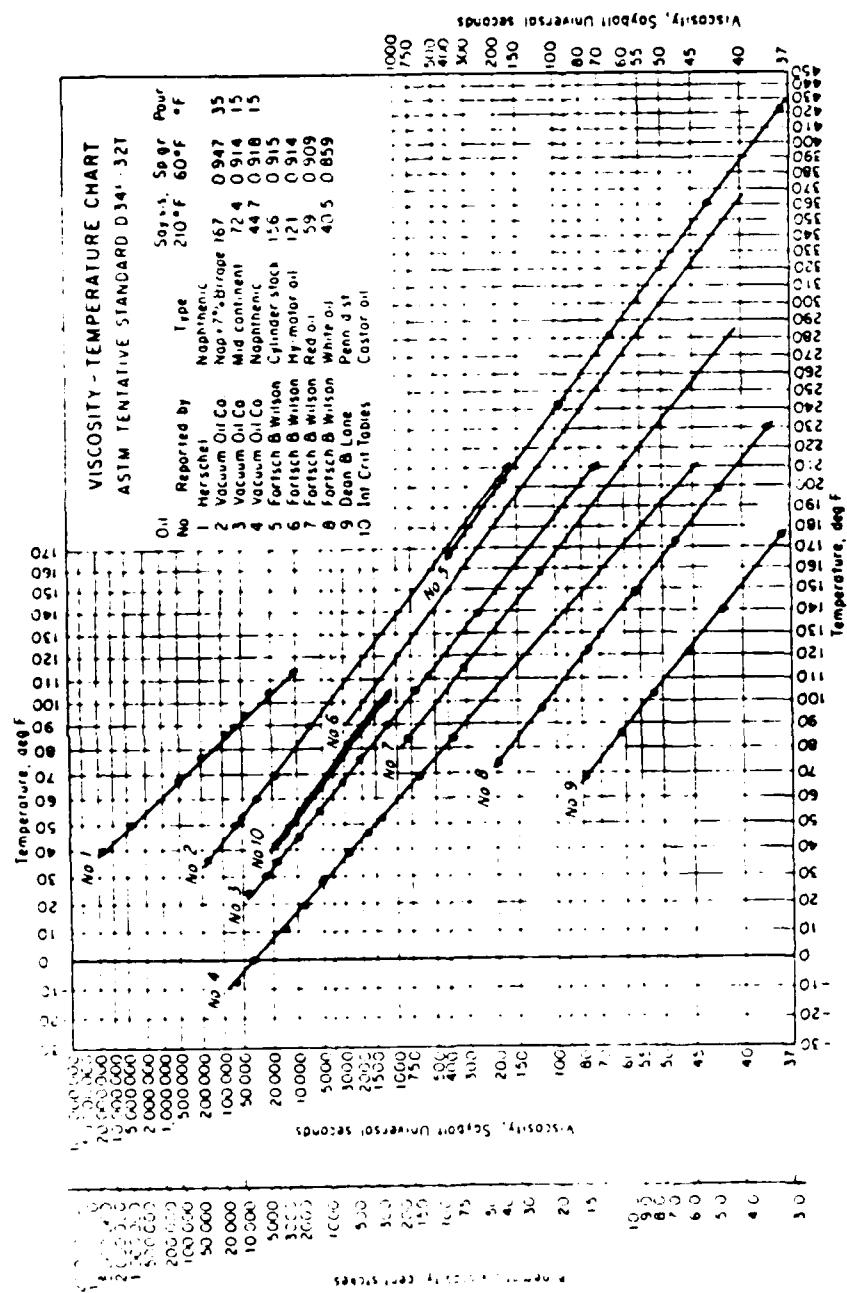
Figure 6. Viscosity-Temperature Chart Showing Typical Experimental Curves

TABLE VI.

AFIT SAE 10W10 Oil Viscosity

Temp.-F	ν - Centistokes	μ - (lbf-sec)/ft²
70	18.80	3.39 X 10⁻⁴
75	17.50	3.15
80	15.75	2.84
85	13.92	2.51
90	12.86	2.32
95	12.07	2.18
100	10.18	1.83
105	9.50	1.71
110	9.00	1.62
115	8.20	1.48
120	7.50	1.35
125	6.90	1.24
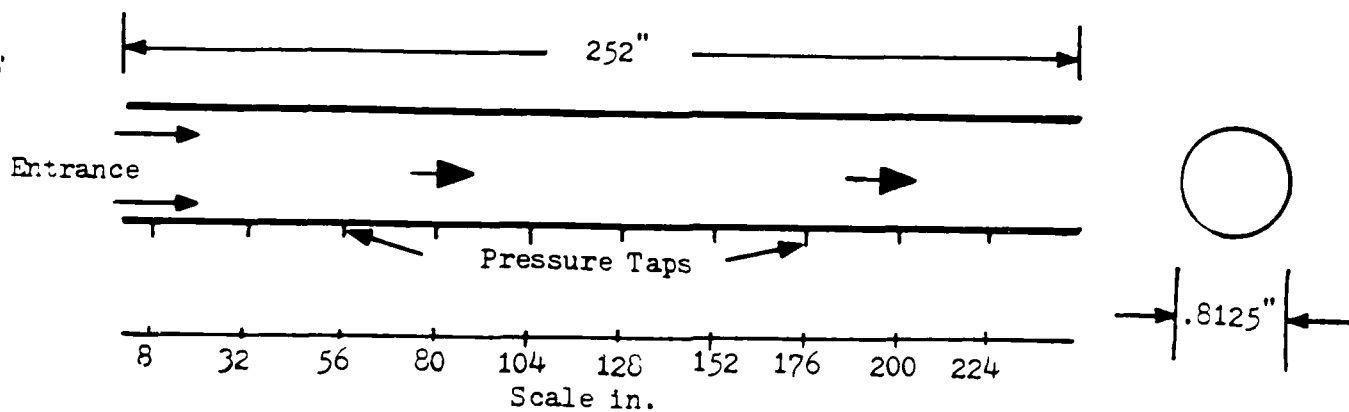
Figure 7.   Circular Duct Diagram

Entrance

Pressure Taps

8   32   56   80   104   128   152   176   200   224

Scale in.

$A = .5185$ in.^{2}

.8125"
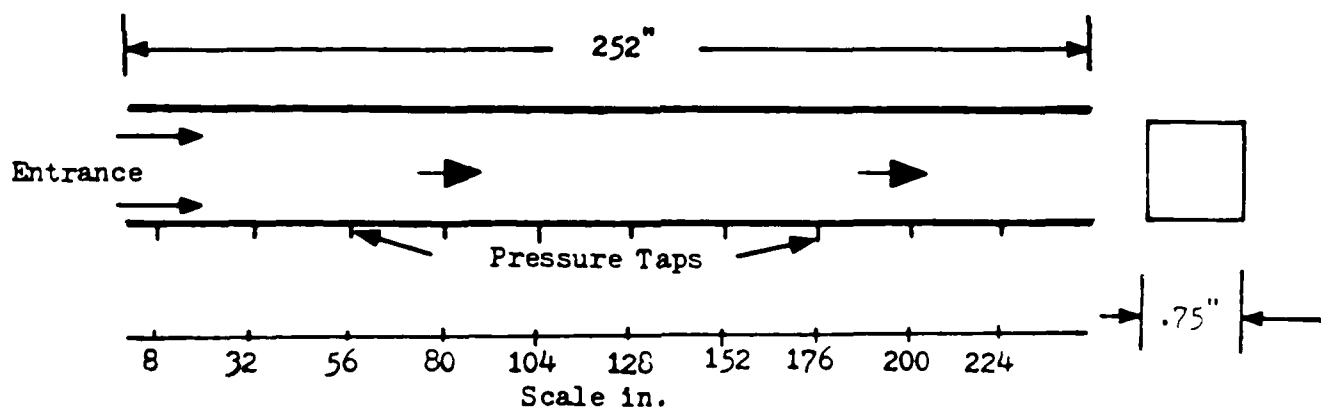
252"

Figure 8.   Square Duct Diagram

Entrance

Pressure Taps

8   32   56   80   104   128   152   176   200   224

Scale in.

$A = .5625$ in.^{2}

.75"

252"

$$r_1/r_2 = .66/.7825 = .8435$$

$$A = .555 \text{ in.}^2$$
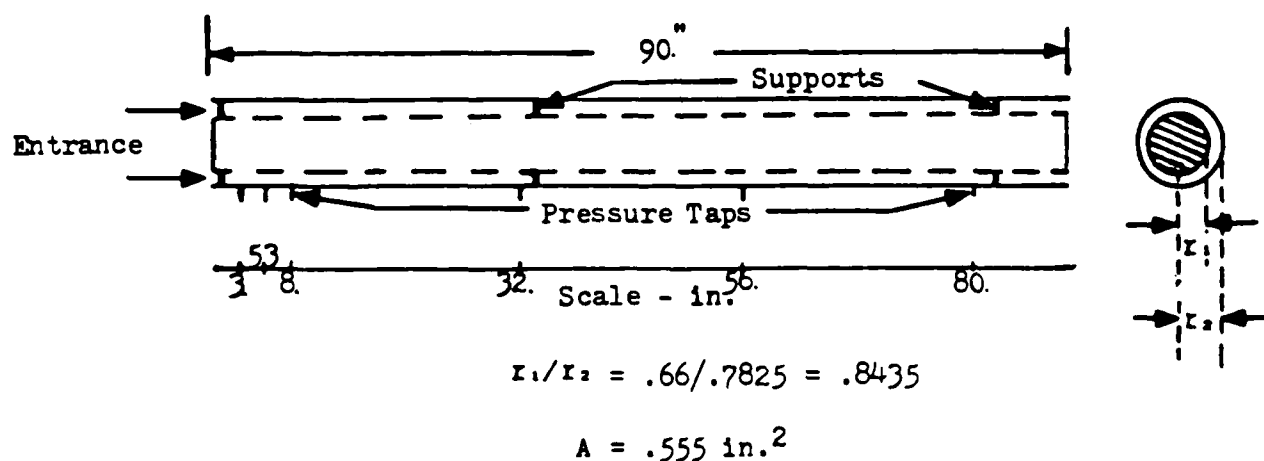
Figure 9. Concentric Annulus Diagram

Concentric Annulus

The concentric annulus, shown in Figure 9, consists of two ducts, one mounted within the other, with $r_1/r_2 =$ .8435. The center duct is blocked at both ends to allow flow between the two ducts only. The concentric annulus was designed to simulate infinite parallel plates flow, which represents the upper bound of $C_f Re$. Figure 10 shows that infinite parallel plates can be simulated with concentric annuli having r_1/r_2 greater than approximately 0.7 (3:286). This duct is 7.5 feet long with a flow height of .1225 inches. This results in a cross-sectional flow area of .555 square inches. Six pressure taps are mounted on the duct with the first three taps located 3.0, 5.3, and 8.0 inches, respectively, downstream of the entrance. the remaining three taps are located every two feet downstream from tap number 3. Since the entrance region developes

27
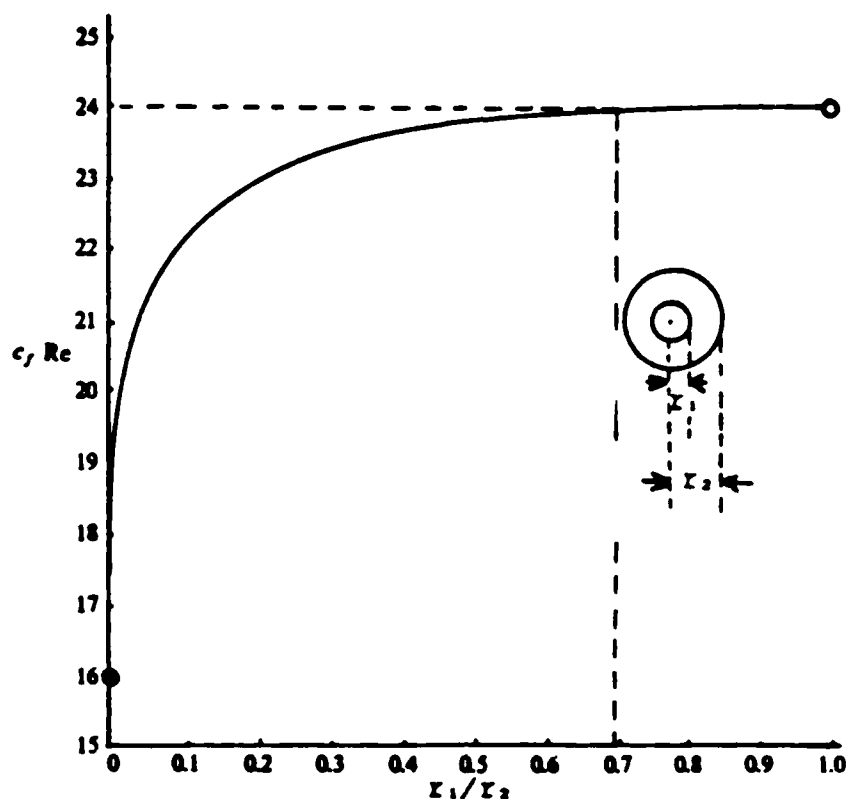
Figure 10.   Friction Factors for Concentric Annuli

quickly for an infinite parallel plate duct, the first
three pressure taps are located as close to the entrance as
possible.

Procedure

The AFIT Oil Flow Rig allows measurement of static
pressure drop along a duct, and the average mass flow rate
through that duct.   With these measurements, and the oil
properties, C_fRe, Re_{tr}, and L^* can be determined.   The
static pressure for each measuring station along the duct

is presented on the mercury manometer board. The weighing

tank is used to measure the mass flow of oil for a specific

time period. By dividing the total mass weighed by the

elapsed time, a mass flow rate can be determined.

$$\dot{m} = \text{lbm oil/time}$$

For friction factor measurements, steady, laminar flow

is established in the duct, and static pressure is recorded

for each of the 10 stations, from the manometer board.

dP/dx is determined from the fully developed (linear)

portion of the pressure curve (see Figure 11). The average

velocity (V), is determined from mass flow rate data where,

$$V = \dot{m}/\rho A$$

Friction factors are then determined from,

$$4C_f = (-dP/dx)(2gD/\rho V^2)$$

Transition from laminar to turbulent flow was

determined visually at the duct exit, with the aid of a

strobotac. Once laminar flow is established in the duct,

the flow velocity was increased until turbulent eddies

become noticable at the duct exit. The strobotac is a

significant aid for this, especially with the concentric

annular duct, where exit flow interaction occurs shortly

past the duct exit. Once this transition point is located,

the selector valve is turned to allow oil to flow into the

weighing tank. The mass flow rate is then determined, and

Re_{tr} calculated as,

$$Re_{tr} = \dot{m}D/A\mu$$

The hydrodynamic entrance length was determined graphically from the pressure vs. position plots for each duct. In fully developed, laminar flow, dP/dx is constant. In the hydrodynamic entrance region, where the velocity profile is still developing, the pressure drop is increasingly greater toward the entrance and thus, non-linear. Where the non-linear portion of the pressure drop curve becomes linear defines X (see Figure 11), and knowing the duct D_h, or $D_{h,l}$, and Re, L^+ can be determined.

P -in. Hg.

dP/dx = C

X

x -in.
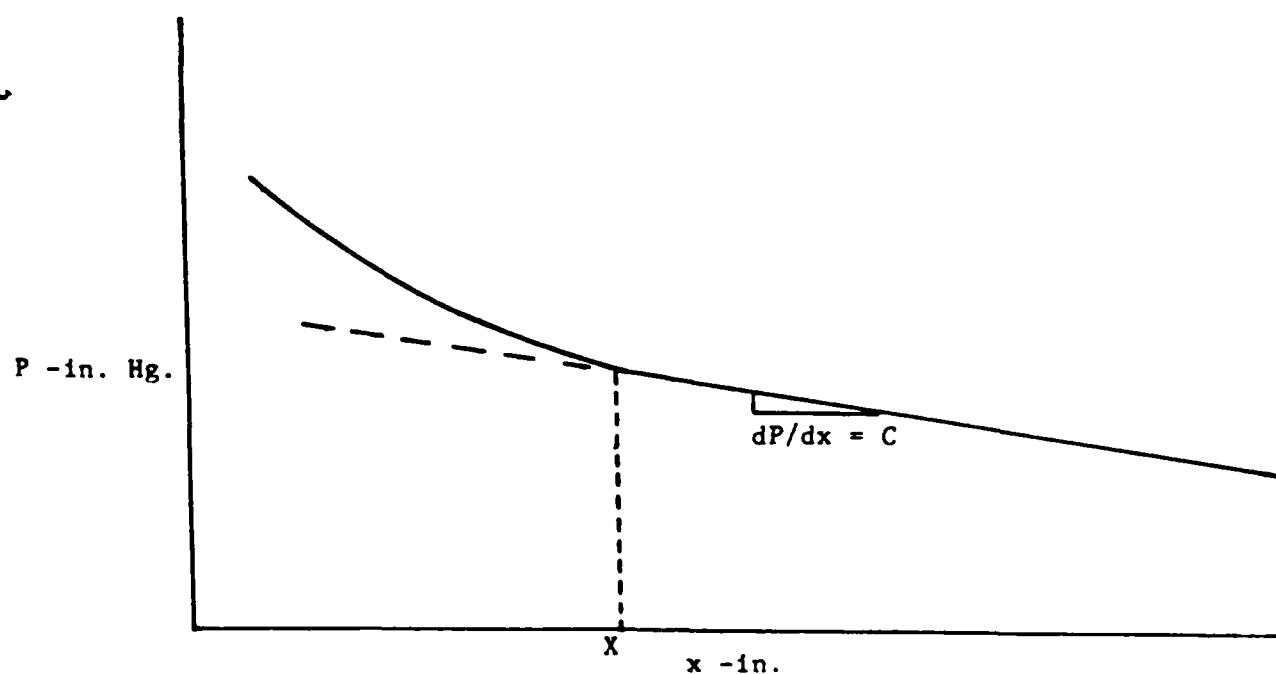
Figure 11. Pressure Drop for Fully Developed, Laminar Flow

V.   Results and Discussion

Friction Factor

Friction factors for each duct can be determined from the pressure drop in the fully developed, laminar flow region. Friction factor data was used to verify exact solutions, based on D_h. Friction factors were determined from,

$$4C_f = (-dP/dx)(2gD/\rho V^2)$$

where D is D_h or $D_{h,i}$, depending on the application.

Friction factor data from the circular, square, and concentric annular ducts are compared to the exact solutions, based on D_h, in Figures 11, 12, and 13, respectively. Pressure and mass flow data are presented in Appendix C, for each duct. The experimental C_f's agree very well with the exact solutions for all three ducts. This is no surprise, since experimental C_f data that verifies the exact solutions is abundant in the literature. More importantly, however, this data provides a high degree of confidence in the data taking and reduction techniques, which carries over to the Re_{tr} and L^* investigations. Since the C_f values, based on D_h, match the analytic exact solutions, by definition, C_f, based on $D_{h,i}$, for the square and concentric annular duct will equal the circular duct value (within the $D_{h,i}$ limitations discussed in section III).

31
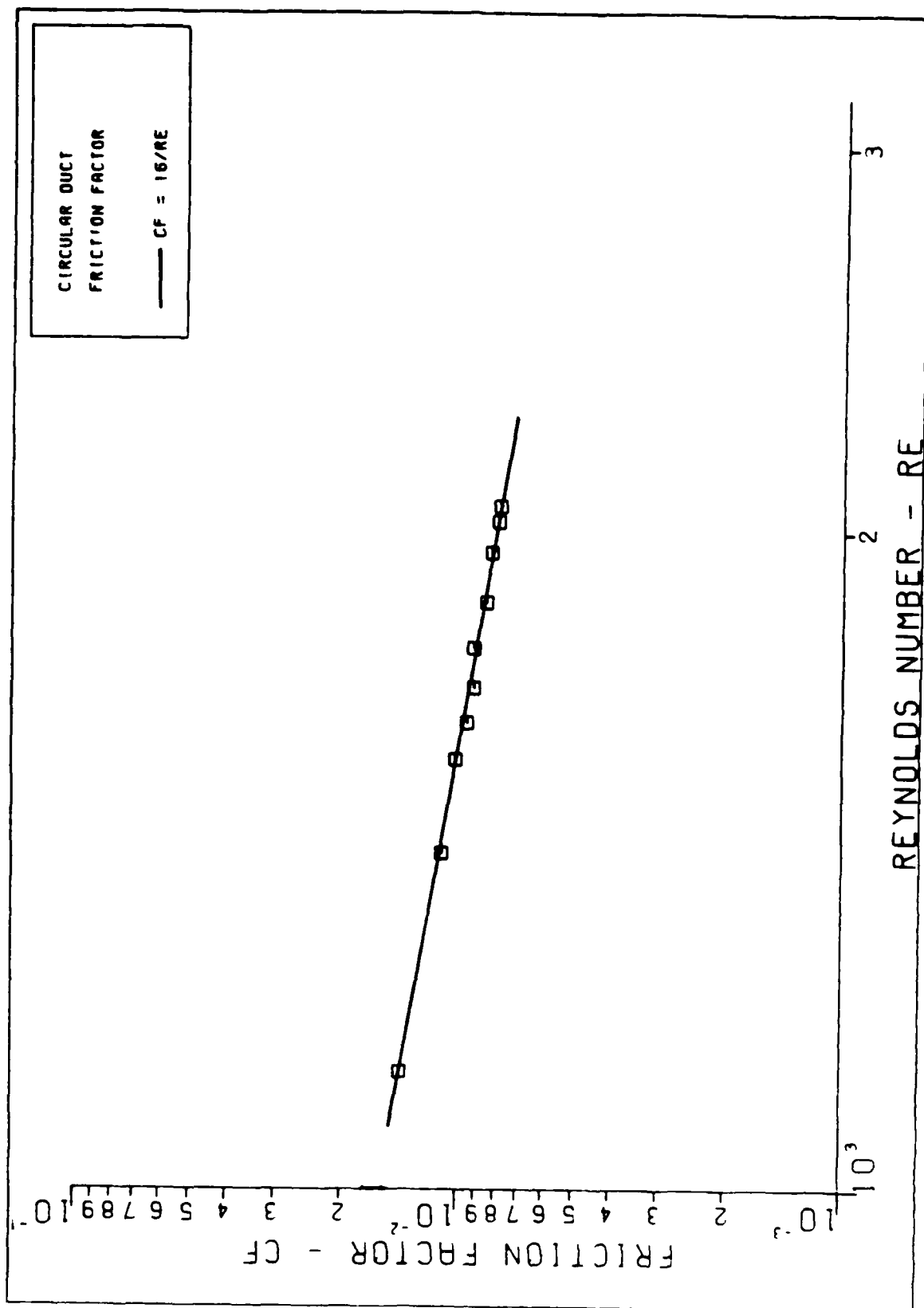
Figure 12. Circular Duct Friction Factors for Fully Developed, Laminar Flow

SQUARE DUCT
FRICTION FACTOR

——— CF = 14.227/RE

REYNOLDS NUMBER - RE
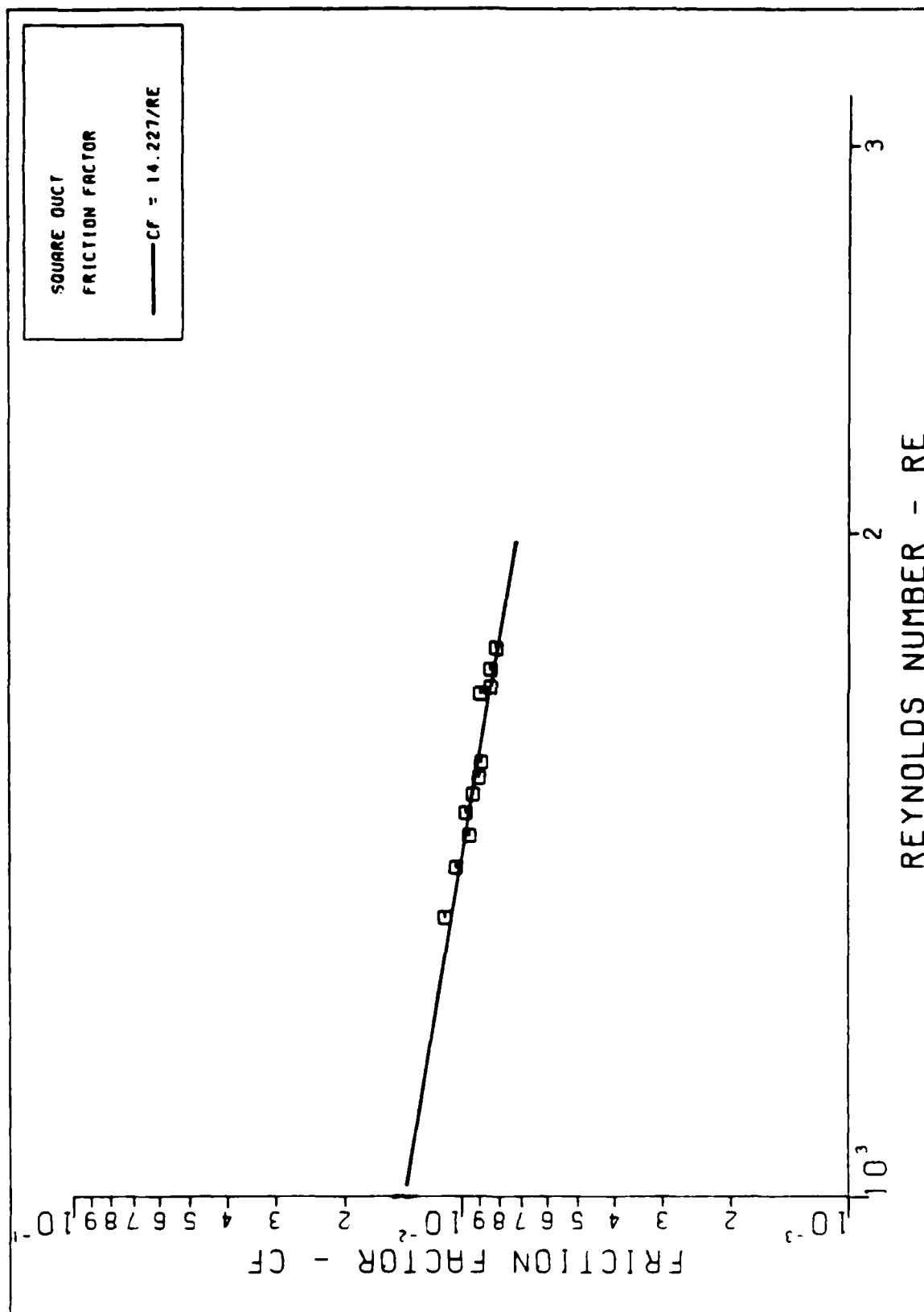
FRICTION FACTOR - CF

Figure 13. Square Duct Friction Factors for Fully Developed, Laminar Flow
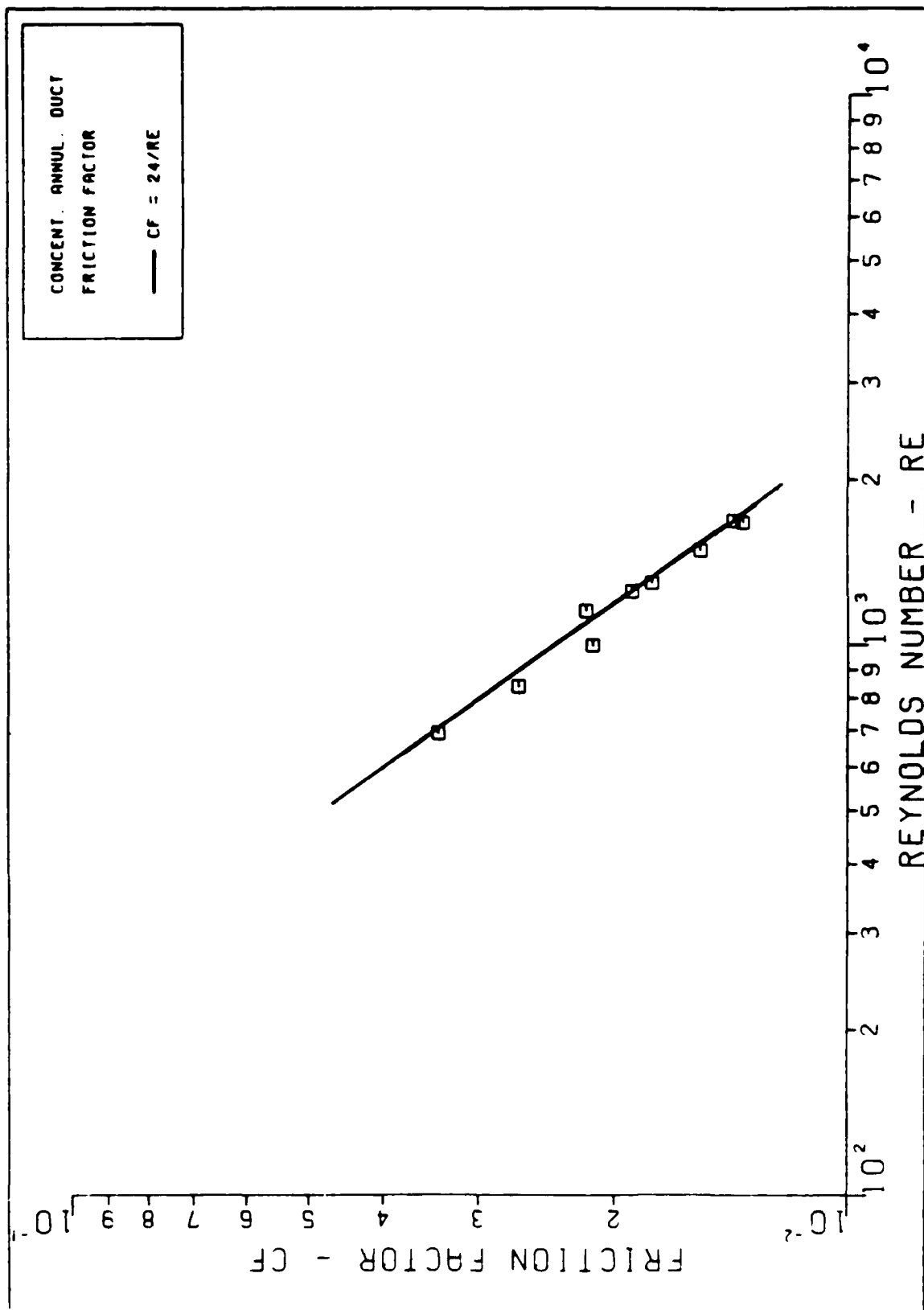
Figure 14. Concentric Annular Friction Factors for Fully Developed, Laminar Flow

Transition Reynolds Number

Transition from laminar to turbulent flow can be precicted, or correlated, by a transition Reynolds number, Re_{tr}. The value for Re_{tr} for circular ducts is approximately 2300. This is only under normal conditions, however. If disturbances in the duct entrance region, as well as the approach to it, are minimized, Re_{tr} can be increased to significantly higher values, the upper limit of which has not been established. V.W. Ekman, for example, reached a Re_{tr} of 40,000 with an exceptionally disturbance free entrance (15). The lower bound is approximately 2000, below which laminar flow is maintained, even with very strong disturbances present (2:433)

This author has found no data on Re_{tr} for non-circular ducts. If the Re_{tr}, based on D_h, is, in fact, dissimilar for different duct shapes, a desirable trait of $D_{h,i}$ would be to correlate the Re_{tr} for all duct shapes to the circular duct value of 2000.

The three ducts each have abrupt entrances which induce a large disturbance at the entrance. With such a disturbance, transition should take place at the minimum Re_{tr} for each duct. For example, historical data indicates that this will occur at Re_{tr} = 2000 for a circular duct. The abrupt entrance should eliminate the Re_{tr} dependence on duct roughness.

Transition Reynolds number, based on $D_{h,1}$, is defined as:

$$Re_{tr,e1} = (\rho VD_h/\mu)(D_{h,1}/D_h)$$

Transition Reynolds number were first calculated based on D_h to compare to the circular duct Re_{tr}. This was done because this author found no data on Re_{tr} for non-circular ducts. The $D_{h,1}$ correction was then applied to try to correlate the data to the circular duct value. For these calculations, μ was taken from Table VI for all three ducts. This was done after the extrapolated values from Table VI were verified from the circular duct data, using the Hagen-Poiseuille law (see Appendix D).

Ten to 15 data runs at transition were made for each of the three ducts, with the average Re_{tr}, based on both D_h and $D_{h,1}$, shown in Table VII. Individual Re_{tr} values can be found in Appendix C. The circular duct Re_{tr} was 2028, which matches the historical value extremely well. The square and concentric annular ducts had Re_{tr}s, based on D_h, approximately 12.5% below the circular duct Re_{tr}. What is interesting to note here is that the square and concentric annular ducts, each have similiar Re_{tr}, even though they are significantly different duct shapes. Recall, these two ducts were chosen because they represented two extremes when considering C_fRe, based on D_h. The new hydraulic diameter appears to work well correlating the square duct

36

TABLE VII

Transition Reynolds Numbers

Duct	$Re_{tr} - D_h$	$Re_{tr} - D_{h,l}$
Circle	2028	2028
Square	1750	1925
Concentric Annulus	1733	1165

Re_{tr} to that of the circular duct. However, for the concentric annular duct, the Re_{tr} diverges from the circular duct value. This data indicates that Re_{tr}, based on D_h, remains the best choice.

Hydrodynamic Entrance Length

Hydrodynamic entrance length is defined as the duct length required to achieve a duct centerline velocity 99% of the fully developed value. The non-dimensional form is

$$L^* = (X/D)/Re$$

where D is either D_h, or $D_{h,i}$, depending on the application. Hydrodynamic entrance length is important in that it represents a position where fully developed flow can be assumed. For a circular duct, Liu (16) calculated $L^* = .0541$, Heaton (17) predicted $L^* = .0575$, and Langhaar (18) calculated $L^* = .058$. For equilateral triangular ducts, Shah (19) reported $L^* = .0398$. Table VIII and Table IX present analytic L^* for rectangular and concentric annular ducts, respectively. From these data it is easily seen that L^* varies considerably from duct shape to shape. In fact, as Table VIII and Table IX show, authors often disagree on L^* for a particular duct geometry. Data in Table VIII and Table IX represent analytic results. Little experimental data exists to verify the most accurate analytic method. This demonstrates the need for a parameter such as $D_{h,i}$ which can correlate data for different duct shapes to the circular duct value.

For each of the three ducts, 10 to 15 laminar flow data runs were made, at various Re, to determine L^* (see Appendix E).

TABLE VIII.
Rectangular Duct L⁺ for Fully Developed Laminar Flow

L^*

$1/\alpha$	Wiginton Dalton (21)	Fleming Sparrow (22)	Han (23)
1	0.090	-	0.0752
0.750	-	-	0.0735
0.500	0.085	0.095	0.0660
0.250	0.075	-	0.0427
0.200	0.080	0.080	-
0.125	-	-	0.0227
0	-	-	0.0099

TABLE IX.

Concentric Annular Duct

L* for Fully Developed Laminar Flow

				$L^{\cdot}$		
r_1/r_2	Liu (16)	Manohar (25)	Roy (26)	Heaton (17)	Coney (27)	Sparrow (28)
0	.0541	-	-	.0575	-	-
0.001	-	-	-	.0296	-	.0375
0.01	-	-	-	-	-	.0303
0.02	-	-	-	.0206	-	-
0.05	.0206	-	-	.0172	.0329	.0241
0.10	.0175	.0164	.0180	.0146	.0253	.0210
0.20	-	-	.0158	-	.0214	.0171
0.25	-	-	-	.0118	.0204	-
0.30	-	.0122	.0140	-	.0194	-
0.40	-	-	.0128	-	.0178	.0131
0.50	.0116	.0110	.0121	.0103	.0168	-
0.60	-	-	.0114	-	.0161	-
0.70	-	.0103	-	-	.0156	-
0.75	.0109	-	-	-	.0152	-
0.80	-	-	.0113	_	.0150	.0118
1.00	.0108	-	-	.0099	.0147	-

TABLE X

Experimental Hydrodynamic Entrance Length

Duct	$L^* - D_h$	$L^* - D_{h,1}$
Circle	.0574	.0574
Square	.0917	.0758
Concentric Annulus	– (.011 - Anal.)	– (.0163 - Anal.)

The experimental L^* values, based on D_h and $D_{h,1}$, are shown in Table X. The hydrodynamic entrance length for the circular and square ducts were easily determined from plots like those shown in Figures 15 and 16, respectively. The concentric annular duct, however, posed some problems. By examining Figure 17, it is seen that the pressure drop stays constant, for the concentric annulur duct, from station 1 to 6, even at high Re. A hydrodynamic developing region is indeterminable from the data, thus making it impossible to graphically determine L^*. By examining the analytic L^* data from Table IX, a possible explanation is found. For $r_1/r_2 = .84$, L^* is approximately .011. For a Re of 1700, just before transition, X, for this duct, is approximately 4.6 inches. Recall the first two pressure taps were located at 3.0 and 5.3 inches downstream of the entrance. The flow is fully developed before it reaches the second pressure tap! To graphically determine L^*, with only the first pressure tap within the hydrodynamic
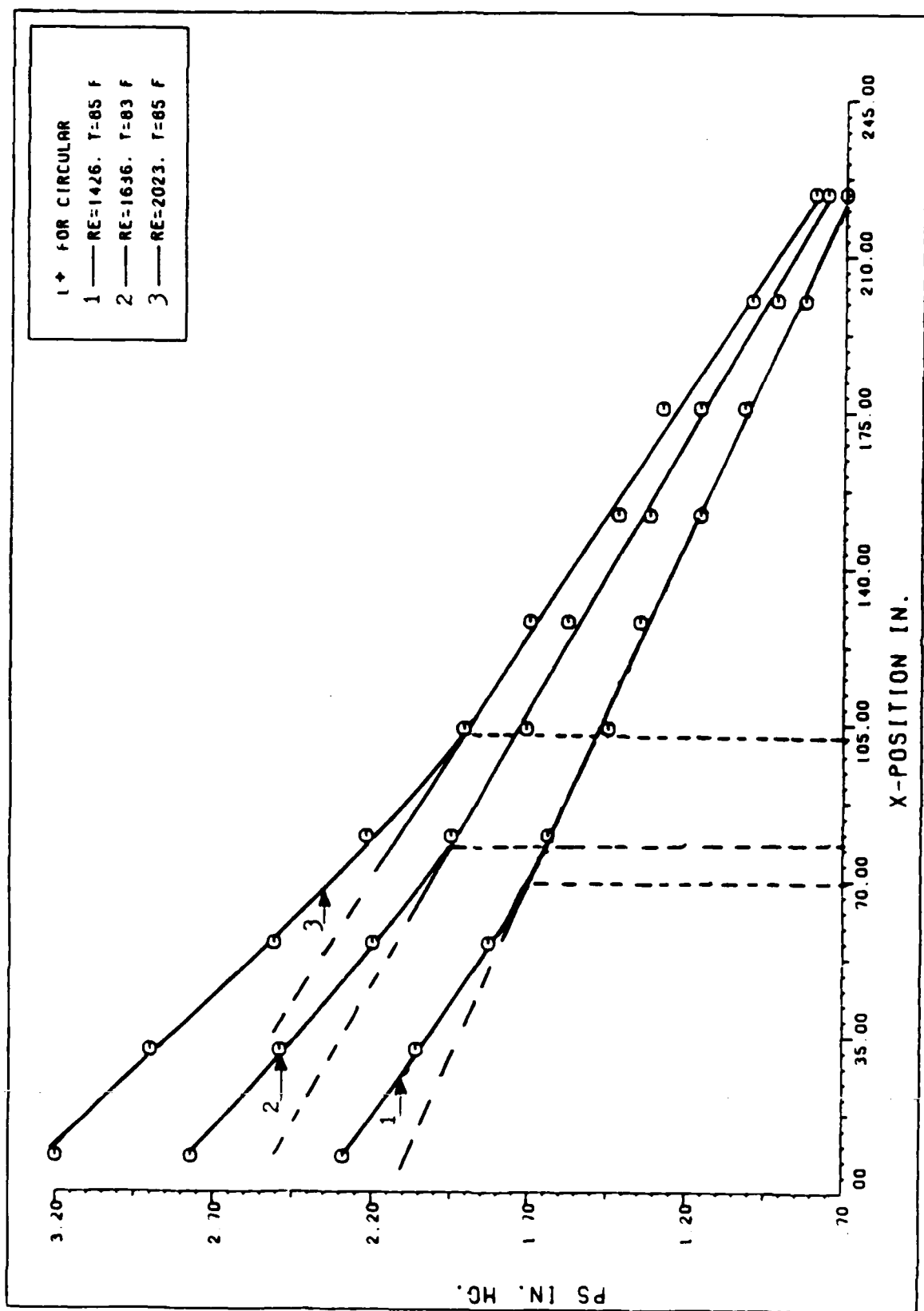
Figure 15. Hydrodynamic Entrance Length for Circular Duct

42
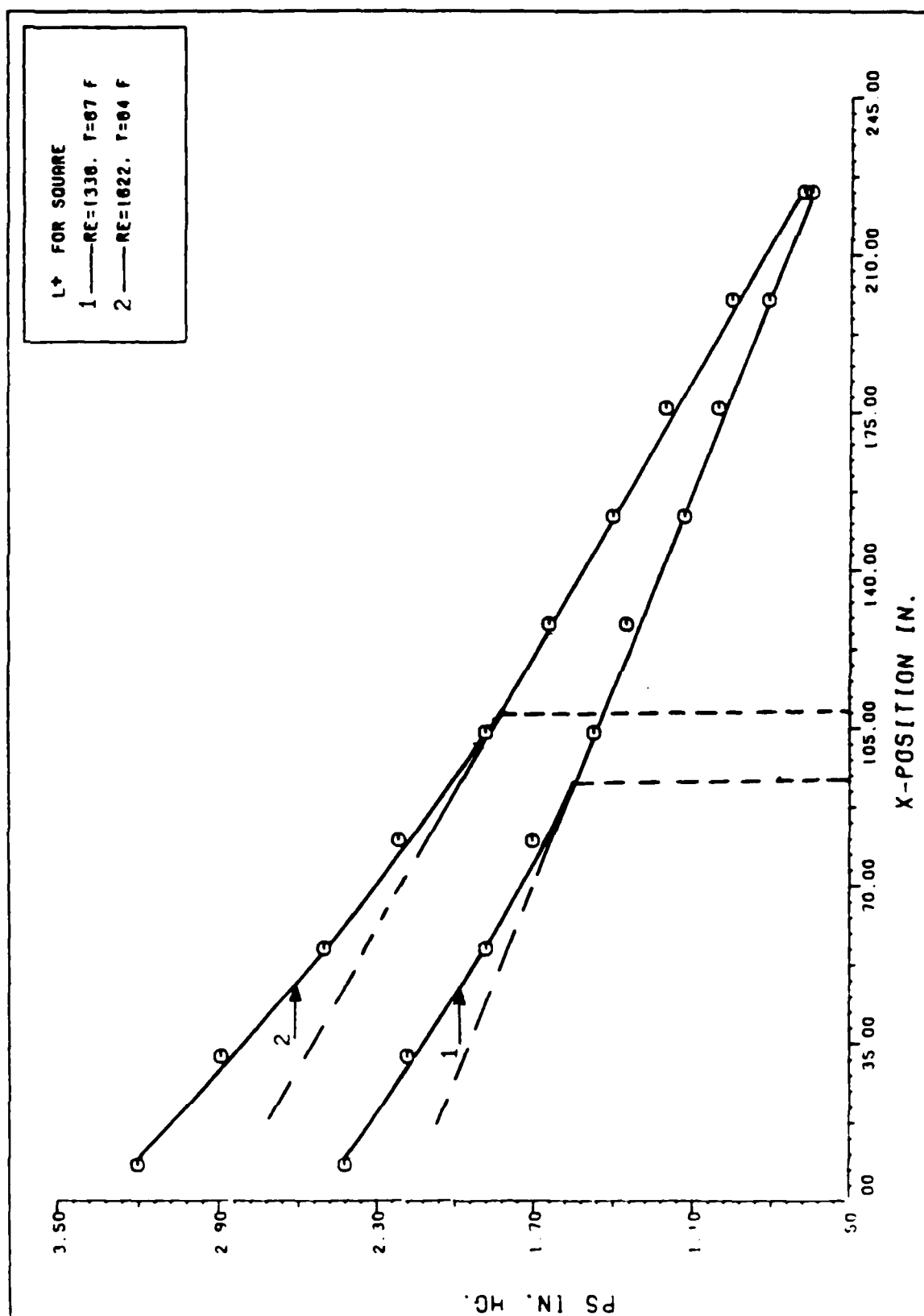
Figure 16. Hydrodynamic Entrance Length for Square Duct
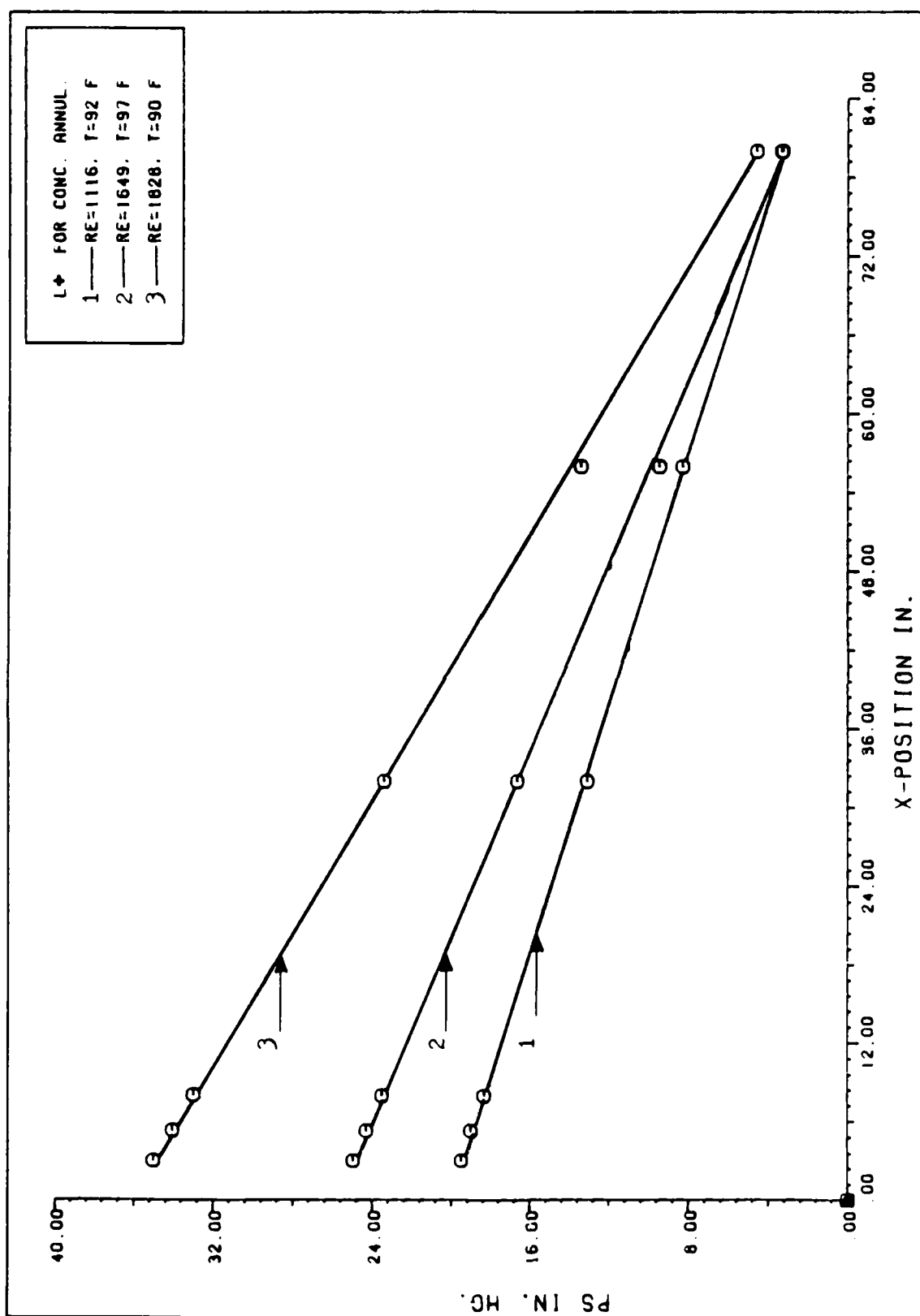
Figure 17. Hydrodynamic Entrance Length for Concentric Annular Duct

entrance region, and close to the end, at that, is
virtually impossible. The first three pressure taps were
located as close to the entrance as physically possible, so
a L* cannot be graphically determined for this particular
duct.

The hydrodynamic entrance length, based on D_h, for the
circular duct was 0.0574 which indicates that Heaton (17)
and Langhaar (18) have good analytic techniques in
predicting L*. The square duct had a L* of 0.0917. This
value indicates that Wiginton and Dalton (21) have the best
analytic technique for determining L* for square ducts.

Using $D_{h,i}$ as the characteristic dimension instead of
D_h, does not correlate the data to the circular duct value.
The correlation trend, however, is favorable. The square
duct L* is reduced toward the circular duct value, while
the concentric annular duct L* is increased.

Since the correlation of L*, based on $D_{h,i}$, produced
unsatisfactory results, perhaps a different approach to the
L* problem is needed. Consider flow through a circular
duct as shown in Figure 18. Here the boundary layer
growth, δ , is generally described as,

$$\delta = C(\nu t)^{.5} \qquad (2:83) \qquad (10)$$

where C is a function of the pressure gradient, dP/dx, and
the transverse velocity, v. We will let time, t, be equal
to x/V, for this problem. (It should be noted that V is
not the actual velocity that the boundary sees from

45
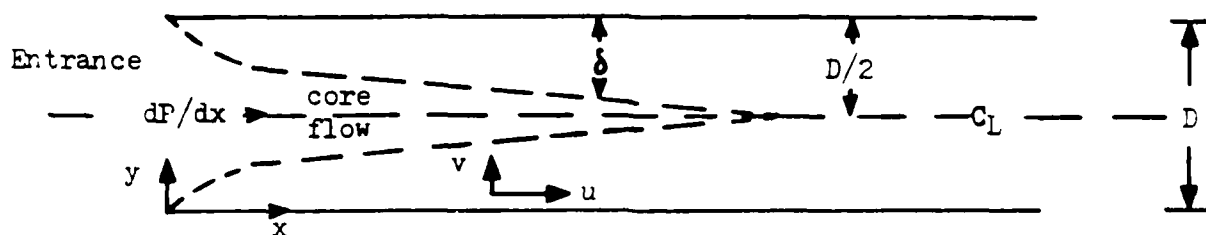
Figure 18. Boundary Layer Growth in the Entrance Region

the entrance to position X. The velocity actually varies,
non-linearly, from V, at the entrance, to 2V, at the
centerline, for a circular duct, but we are using V here
for convenience and to obtain "ballpark" expressions for
L*.) The hydrodynamic entrance length, X, becomes
approximately the position where the boundary layer meets
the duct centerline, δ = D/2. Equation (10) becomes,

$$D/2 = C(\nu X/V)^{.5}$$

which can be rewritten,

$$X/D = (VD/\nu)(1/4C^2) \qquad (11)$$

where $X \propto D^2$.

$$L^* = (X/D)/Re = 1/4C^2 \qquad (12)$$

For the circular duct, L* = .0574, and C is approximately
2.1.

Now let us keep C constant at 2.1, and examine L* for
non-circular ducts, where δ becomes the average distance a
disturbance must travel to reach the duct centerline. Let

46
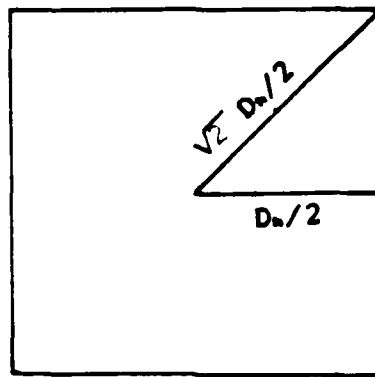
Figure 19. A Square Duct

us examine a square duct, shown in Figure 19, for instance, where, from the corners, a disturbance must travel $(2^{.5})(D_h/2)$ to reach the centerline. For non-circular ducts, X is proportional to D_h^2, so,

$$L^* = (2)(.0574) = .1148$$

This would be the predicted L^* if all the disturbances in a square duct, travelled $(2^{.5})(D_h/2))$ to the center. Obviously this is not the case. Those in the corners travel $(2^{.5})(D_h/2)$, but those on the sides only travel $(D_h/2)$ to the centerline. So, perhaps, the average distance a disturbance travels in a square duct is somewhere between these two values, say at $(1.5)^{.5}(D_h/2)$, for instance. If this is the case,

$$L^* = (1.5)(.0574) = .0861$$

This L^* is very close to our experimental value, $L^* = .0917$! Likewise, for an infinite parallel plate duct, the average disturbance travel distance is $.5(D_h/2)$, so,

$$L^* = .01435$$

47

This also is quite close to the analytically predicted L^* for the infinite parallel plate duct!

So, perhaps, a better way to correlate L^* data would be to scale the constant, C, with a new hydraulic diameter that estimates the average boundary layer growth to the centerline of non-circular ducts.

VI.   Conclusions and Recommendations

Conclusions

In this investigation, a new hydraulic diameter, $D_{h,1}$, that better represented the mean center to surface distance for laminar flow in non-circular ducts was empirically determined. Experimentation was performed to examine the effect on Re_{tr} and L^* of replacing the traditional hydraulic diameter, D_h, with $D_{h,1}$. The experiment was performed using a circular duct, square duct, and concentric annular duct that simulated flow between infinite parallel plates.

The new hydraulic diameter equation correlated C_fRe data to the circular duct value for many non-circular duct shapes. All the shapes examined correlate within 2.4 percent of the circular duct value, with most within 1.5 percent.

Experimental Re_{tr} were obtained for the circular, square, and concentric annular ducts. The circular duct Re_{tr}, based on D_h, was very close to 2000 with the square and concentric annulus Re_{tr} approximately 12.5 percent lower than this value. Square duct Re_{tr}, based on $D_{h,1}$, correlated very close to the circular duct, but the concentric annulus Re_{tr} did not. Concentric annulus Re_{tr} actually diverged from the circular duct Re_{tr}. Based on this data, it appears that $D_{h,1}$, which correlates C_fRe data

49

very well, is not a good characteristic dimension for Re_{tr}. Perhaps an entirely different hydraulic diameter is needed if Re_{tr} is to be correlated to the circular duct value.

Hydrodynamic entrance lengths were determined for only the circular and square ducts. The concentric annular duct flow became fully developed before the second static pressure tap, making accurate prediction of L^* almost impossible. The analytic L^* value for the concentric annulus was thus used for $D_{h,i}$ correlations. Hydrodynamic entrance lenghts, based on $D_{h,i}$, did not correlate well to the circular duct value. The correlation did, however, display the correct trend toward the circular duct value, and, perhaps, multiplication of $D_{h,i}$ by some constant might bring the L^* values in line.

The new hydraulic diameter is quite accurate in correlating $C_f Re$ data, but cannot be relied upon to correlate Re_{tr} and L^* data. Transition Reynolds numbers, based on D_h, were determined for the ducts, and will be useful, since no data for non-circular duct, Re_{tr}, has been reported. Likewise, experimental circular and square duct L^* values, based on D_h, will add to the limited data base available.

Recommendations

The new hydraulic diameter did not correlate Re_{tr} and L^* data. Separate hydraulic diameters are needed to correlate both Re_{tr} and L^* data. The L^* correlation

appears to require only a multiplier applied to the $D_{h,i}$ definition.

Instead of using $D_{h,i}$ directly in the L^* correlation, perhaps determining a $D_{h,i}$ that correlated the constant, C, in the boundary layer growth equation (Equation (10)),would yeild better results, and should be investigated further.

Pressure gages, located close to the static pressure taps, should be installed, instead of relying on the 10-foot pressure lines that currently lead to the manometer board. This would provide better response indications to the pressure fluctuations which indicate the onset of transition. In addition, a static pressure tap should be added to each duct at the exit. This would aid in the detection of flow transition.

Static pressure taps should be installed very close to the entrance of the concentric annular duct to help in the L^* determination. This will require a major material overhaul.

Unusual duct shapes, such as triangular, hexagonal, or semi-circular, should be used in the investigation of $C_f Re$, Re_{tr}, and L^*, to increase the experimental data base used in the $D_{h,i}$ correlations. It would be interesting to see where the data for these ducts fall, compared to that of the square and concentric annulus.

New Hydraulic Diameter Calculations

Notation:

A = Duct area

P = Duct perimeter

Ac = Area of the modelling circle

Pc = Perimeter of the modelling circle

Ae = A - Ac

Pe = P + Pc

W = Width of infinite parallel plates (approaches infinity)

TABLE XI.

Compact Duct Hydraulic Diameters

Shape	A	P	Ac	Pc	Ae	Pe	Ae/Pe	$D_{h,i}$	D_h
Circle	$.78S^2$	3.14S	$.78S^2$	3.14S	$.00S^2$	6.28S	.000S	1.00S	1.00S
Square	$1.0S^2$	4.00S	$.78S^2$	3.14S	$.21S^2$	7.14S	.031S	1.10S	1.00S
Triang	$.43S^2$	3.00S	$.26S^2$	1.81S	$.17S^2$	4.81S	.036S	.693S	.577S
Hexag	$2.6S^2$	6.00S	$2.4S^2$	5.44S	$.24S^2$	11.4S	.021S	1.80S	1.73S
Semi-Circle	$.40S^2$	2.57S	$.26S^2$	1.80S	$.14S^2$	4.37S	.033S	.633S	.611S

Infinite   A = WS   P = 2W + 2S
Parallel
Plates   Ac = .79WS   Pc = 2W

            Ae = .21WS   Pe = 4W + 2S   Ae/Pe = .21WS/(4W+2S)

As W goes to infinity, Ae/Pe reduces to .05365S

            $D_{h,i}$ = 1.34S D_h = 2S

TABLE XII.

Rectangular Hydraulic Diameters

a	A	P	Ac	Pc	Ae	Pe	Ae/Pe	D_{h1}	D_h
1.00	$1.00S^2$	$4.0S$	$0.79S^2$	$3.0S$	$0.21S^2$	$7.0S$	.031S	1.10S	1.00S
1.25	$1.25S^2$	$4.5S$	$0.98S^2$	$3.4S$	$0.27S^2$	$7.9S$	.034S	1.24S	1.11S
1.50	$1.50S^2$	$5.0S$	$1.18S^2$	$3.9S$	$0.32S^2$	$8.9S$	.036S	1.29S	1.20S
1.75	$1.75S^2$	$5.5S$	$1.37S^2$	$4.3S$	$0.38S^2$	$9.8S$	.038S	1.33S	1.27S
2.00	$2.00S^2$	$6.0S$	$1.57S^2$	$4.8S$	$0.43S^2$	$10.8S$	.040S	1.35S	1.33S
2.25	$2.25S^2$	$6.5S$	$1.77S^2$	$5.3S$	$0.48S^2$	$11.8S$	.041S	1.37S	1.38S
2.50	$2.50S^2$	$7.0S$	$1.96S^2$	$5.7S$	$0.54S^2$	$12.7S$	.042S	1.38S	1.43S
2.75	$2.75S^2$	$7.5S$	$2.16S^2$	$6.2S$	$0.59S^2$	$13.7S$	.043S	1.39S	1.47S
3.00	$3.00S^2$	$8.0S$	$2.36S^2$	$6.7S$	$0.64S^2$	$14.7S$	.044S	1.39S	1.50S
3.25	$3.25S^2$	$8.5S$	$2.55S^2$	$7.2S$	$0.70S^2$	$15.7S$	.044S	1.40S	1.53S
3.50	$3.50S^2$	$9.0S$	$2.75S^2$	$7.7S$	$0.75S^2$	$16.7S$	.045S	1.40S	1.56S
3.75	$3.75S^2$	$9.5S$	$2.95S^2$	$8.2S$	$0.80S^2$	$17.7S$	.045S	1.40S	1.58S
4.00	$4.00S^2$	$10.0S$	$3.14S^2$	$8.7S$	$0.86S^2$	$18.7S$	.046S	1.40S	1.60S
4.25	$4.25S^2$	$10.5S$	$3.34S^2$	$9.2S$	$0.91S^2$	$19.7S$	.046S	1.40S	1.62S
4.50	$4.50S^2$	$11.0S$	$3.53S^2$	$9.7S$	$0.97S^2$	$20.7S$	.047S	1.40S	1.64S
4.75	$4.75S^2$	$11.5S$	$3.73S^2$	$10.2S$	$1.02S^2$	$21.7S$	.047S	1.41S	1.65S
5.00	$5.00S^2$	$12.0S$	$3.93S^2$	$10.7S$	$1.07S^2$	$22.7S$	.047S	1.41S	1.67S
5.25	$5.25S^2$	$12.5S$	$4.12S^2$	$11.2S$	$1.13S^2$	$23.7S$	.048S	1.40S	1.68S
5.50	$5.50S^2$	$13.0S$	$4.32S^2$	$11.6S$	$1.18S^2$	$24.6S$	.048S	1.40S	1.69S
5.75	$5.75S^2$	$13.5S$	$4.52S^2$	$12.1S$	$1.23S^2$	$25.6S$	.048S	1.40S	1.70S
6.00	$6.00S^2$	$14.0S$	$4.71S^2$	$12.6S$	$1.29S^2$	$26.6S$	.048S	1.40S	1.71S
6.25	$6.25S^2$	$14.5S$	$4.91S^2$	$13.1S$	$1.34S^2$	$27.6S$	.049S	1.40S	1.72S
6.50	$6.50S^2$	$15.0S$	$5.11S^2$	$13.6S$	$1.39S^2$	$28.6S$	.049S	1.40S	1.73S
6.75	$6.75S^2$	$15.5S$	$5.30S^2$	$14.0S$	$1.45S^2$	$29.5S$	.049S	1.40S	1.74S
7.00	$7.00S^2$	$16.0S$	$5.50S^2$	$14.5S$	$1.50S^2$	$30.5S$	.049S	1.40S	1.75S
7.25	$7.25S^2$	$16.5S$	$5.69S^2$	$15.0S$	$1.56S^2$	$31.5S$	.049S	1.40S	1.76S
7.50	$7.50S^2$	$17.0S$	$5.89S^2$	$15.5S$	$1.61S^2$	$32.5S$	.050S	1.40S	1.76S
7.75	$7.75S^2$	$17.5S$	$6.09S^2$	$15.9S$	$1.66S^2$	$33.4S$	.050S	1.40S	1.77S
8.00	$8.00S^2$	$18.0S$	$6.28S^2$	$16.4S$	$1.72S^2$	$34.4S$	.050S	1.40S	1.78S
8.25	$8.25S^2$	$18.5S$	$6.48S^2$	$16.8S$	$1.77S^2$	$35.3S$	.050S	1.40S	1.78S
8.50	$8.50S^2$	$19.0S$	$6.68S^2$	$17.3S$	$1.82S^2$	$36.3S$	.050S	1.40S	1.79S
8.75	$8.75S^2$	$19.5S$	$6.87S^2$	$17.8S$	$1.88S^2$	$37.3S$	.050S	1.40S	1.79S
9.00	$9.00S^2$	$20.0S$	$7.07S^2$	$18.2S$	$1.93S^2$	$38.2S$	.051S	1.40S	1.80S
9.25	$9.25S^2$	$20.5S$	$7.26S^2$	$18.7S$	$1.99S^2$	$39.2S$	.051S	1.40S	1.80S
9.50	$9.50S^2$	$21.0S$	$7.46S^2$	$19.1S$	$2.04S^2$	$40.1S$	.051S	1.40S	1.81S
9.75	$9.75S^2$	$21.5S$	$7.66S^2$	$19.6S$	$2.09S^2$	$41.1S$	.051S	1.40S	1.81S
10.00	$10.00S^2$	$22.0S$	$7.85S^2$	$20.0S$	$2.15S^2$	$42.0S$	.051S	1.40S	1.82S
25.00	$25.00S^2$	$52.0S$	$9.64S^2$	$50.0S$	$5.37S^2$	$102.0S$	.053S	1.37S	1.92S
50.00	$50.00S^2$	$102.0S$	$39.3S^2$	$100.0S$	$10.7S^2$	$202.0S$	.053S	1.36S	1.96S
100.0	$100.0S^2$	$202.0S$	$78.5S^2$	$200.0S$	$21.5S^2$	$402.0S$	.053S	1.35S	1.98S

Appendix B.

Specific Gravity Measurements

TABLE XIII.

AFIT SAE 10W10 Oil Specific Gravity Measurements

Measurement	Water (grams)	Oil (grams)	Sp. Gr.
1	198.3	168.3	.849
2	377.0	325.6	.864
3	432.0	373.0	.8635
4	482.1	417.0	.8652
5	482.8	423.0	.876
6	541.2	466.4	.862
AVERAGE			.863

Appendix C.

Data Reduction

TABLE XIV.

Data for Circular Duct, Laminar Flow

Run Number

	1	2	3	4	5	6
P_1 - in. Hg	3.20	2.77	2.29	1.92	2.14	2.24
P_2	2.83	2.49	2.06	1.78	1.92	2.00
P_3	2.53	2.20	1.83	1.60	1.72	1.78
P_4	2.25	1.95	1.64	1.45	1.50	1.55
P_5	1.97	1.71	1.45	1.25	1.35	1.39
P_6	1.78	1.58	1.35	1.19	1.28	1.29
P_7	1.48	1.32	1.16	1.01	1.09	1.10
P_8	1.28	1.16	1.02	0.97	0.98	0.99
P_9	1.02	0.92	0.83	0.78	0.80	0.80
P_{10}	0.76	0.74	0.70	0.69	0.70	0.70
Temp - F	81.0	83.0	85.0	87.5	92.0	93.0
$\dot{m}$ - lbm/sec	0.84	0.74	0.61	0.49	0.61	0.65
V - ft/sec	4.33	3.82	3.16	2.53	3.15	3.35
C_f	.0366	.0380	.0440	.0560	.0405	.0365
RE	1770	1636	1426	1132	1574	1698

TABLE XV.

Data for Circular Duct, Transition Flow
Data Set 1

Run Number

	1	2	3	4	5	6
P_1 - in. Hg	3.20	2.89	2.90	2.80	2.51	2.30
P_2	2.90	2.60	2.61	2.50	2.23	2.04
P_3	2.51	2.27	2.29	2.22	2.00	1.81
P_4	2.22	2.02	2.02	1.96	1.78	1.60
P_5	1.91	1.75	1.73	1.73	1.56	1.40
P_6	1.70	1.60	1.61	1.55	1.40	1.30
P_7	1.42	1.32	1.34	1.30	1.10	1.11
P_8	1.28	1.19	1.18	1.15	1.03	1.01
P_9	1.00	0.91	0.93	0.92	0.86	0.83
P_{10}	0.80	0.79	0.79	0.74	0.72	0.71
Temp - F	84.8	86.7	88.0	90.0	92.1	94.8
$\dot{m}$ - lbm/sec	0.88	0.82	0.81	0.80	0.79	0.74
V - ft/sec	4.51	4.23	4.15	4.13	4.05	3.83
C_f	.0316	.0330	.0339	.0324	.0307	.0295
RE	2023	1958	1962	2014	2027	1976

56

TABLE XVI.

Data for Circular Duct, Transition Flow
Data Set 2

<u>Run Number</u>

	1	2	3	4	5	6
P_1 - in. Hg	4.00	3.90	3.40	3.22	3.12	2.15
P_2	3.56	3.50	3.04	2.91	2.85	1.95
P_3	3.15	3.05	2.66	2.57	2.50	1.75
P_4	2.83	2.70	2.40	2.20	2.17	1.58
P_8	2.41	2.32	2.05	1.91	1.85	1.39
P_6	2.14	2.00	1.82	1.75	1.70	1.28
P_7	1.78	1.67	1.55	1.45	1.46	1.10
P_8	1.47	1.43	1.32	1.25	1.2	1:00
P_9	1.15	1.11	1.04	1.00	1.00	0.82
P_{10}	0.85	0.81	0.80	0.80	0.73	0.70
Temp - F	81.0	82.5	85.5	89.0	91.0	96.5
$\dot{m}$ - lbm/sec	1.02	1.00	0.90	0.83	0.80	0.66
V - ft/sec	5.26	5.16	4.62	4.28	4.13	3.40
C_f	.0321	.0323	.0322	.0312	.0316	.0340
RE	2149	2183	2098	2056	2038	1858

TABLE XVII.

Data for Square Duct, Laminar Flow
Data Set 1

<u>Run Number</u>

	1	2	3	4	5	6
P_1 - in. Hg	2.42	1.71	2.49	2.05	2.73	2.33
P_2	2.18	1.55	2.21	1.86	2.44	2.10
P_3	1.88	1.35	1.93	1.61	2.12	1.81
P_4	1.70	1.25	1.79	1.50	1.95	1.70
P_5	1.47	1.11	1.50	1.26	1.64	1.42
P_6	1.35	1.06	1.39	1.17	1.50	1.31
P_7	1.13	0.90	1.16	1.00	1.25	1.13
P_8	1.00	0.85	1.04	0.90	1.11	1.02
P_9	0.81	0.73	0.85	0.76	0.90	0.86
P_{10}	0.65	0.66	0.70	0.65	0.67	0.68
Temp - F	87.0	97.3	88.0	94.0	83.5	90.0
$\dot{m}$ - lbm/sec	0.66	0.52	0.70	0.65	0.74	0.68
V - ft/sec	3.11	2.47	3.33	3.07	3.52	3.23
C_f	.0441	.0378	.0381	.0343	.0412	.0381
RE	1338	1281	1453	1453	1410	1458

TABLE XVIII.

Data for Square Duct, Laminar Flow
Data Set 2

Run Number

	1	2	3
P_1 -in. Hg	1.71	1.77	3.50
P_2	1.55	1.60	3.12
P_3	1.38	1.41	2.69
P_4	1.31	1.30	2.39
P_5	1.13	1.13	2.04
P_6	1.09	1.08	1.81
P_7	0.92	0.90	1.50
P_8	0.86	0.87	1.30
P_9	0.74	0.73	1.04
P_{10}	0.62	0.62	0.72
Temp - F	100.	100.	78.0
$\dot{m}$ - lbm/sec	0.56	0.57	0.89
V - ft/sec	2.66	2.71	4.23
C_f	.0373	.0360	.0389
RE	1522	1549	1493

TABLE XIX.

Data for Square Duct, Transition Flow
Data Set 1

Run Number

	1	2	3	4	5	6
P_1 - in. Hg	3.00	3.00	3.20	3.00	2.90	2.73
P_2	2.71	2.67	2.89	2.65	2.60	2.45
P_3	2.32	2.31	2.50	2.30	2.25	2.11
P_4	2.05	2.11	2.21	2.08	2.02	1.90
P_5	1.75	1.75	1.88	1.72	1.68	1.61
P_6	1.59	1.58	1.64	1.55	1.52	1.41
P_7	1.28	1.30	1.40	1.30	1.28	1.20
P_8	1.13	1.14	1.20	1.14	1.12	1.08
P_9	0.91	0.93	0.95	0.93	0.91	0.88
P_{10}	0.77	0.70	0.68	0.67	0.70	0.60
Temp - F	90.5	89.0	84.0	86.8	88.0	92.7
$\dot{m}$ - lbm/sec	0.83	0.84	0.84	0.83	0.82	0.80
V - ft/sec	3.96	3.99	3.99	3.95	3.90	3.80
C_f	.0286	.0337	.0397	.0356	.0336	.0325
RE	1797	1772	1622	1691	1702	1773

60

TABLE XX.

Data for Square Duct, Transition Flow
Data Set 2

Run Number

	1	2	3	4	5	6
P_1 - in. Hg	4.16	3.31	2.94	2.49	2.08	2.16
P_2	3.70	2.95	2.63	2.24	1.87	1.94
P_3	3.25	2.60	2.23	1.97	1.63	1.72
P_4	2.88	2.30	2.04	1.77	1.50	1.58
P_5	2.40	1.90	1.72	1.49	1.25	1.31
P_6	2.19	1.72	1.56	1.33	1.18	1.20
P_7	1.70	1.45	1.28	1.14	1.00	1.05
P_8	1.47	1.21	1.13	1.02	0.91	0.91
P_9	1.13	0.98	0.90	0.85	0.76	0.78
P_{10}	0.80	0.70	0.65	0.65	0.62	0.65
Temp - F	80.0	86.0	90.0	95.0	100.	100.
$\dot{m}$ - lbm/sec	1.02	0.90	0.83	0.76	0.66	0.69
V - ft/sec	4.85	4.28	3.95	3.61	3.14	3.28
C_f	.0359	.0361	.0356	.0337	.0340	.0327
RE	1786	1811	1779	1734	1794	1875

TABLE XXI.

Data for Concentric Annular Duct, Laminar Flow
Data Set 1

Run Number

	1	2	3	4	5	6
P_1 - in. Hg	28.58	30.24	19.48	23.18	20.94	24.70
P_2	27.80	29.41	19.00	22.60	20.44	24.09
P_3	26.61	28.18	18.32	21.80	19.75	23.40
P_4	19.23	20.26	13.11	15.50	14.15	16.60
P_5	11.12	11.50	8.30	8.30	7.99	9.27
P_6	3.79	3.97	2.23	3.29	2.90	3.36
Temp - F	90.0	92.0	91.8	93.5	96.3	88.0
$\dot{m}$ - lbm/sec	2.12	2.33	1.54	1.86	1.89	1.80
V - ft/sec	10.2	11.2	7.42	8.94	9.10	8.67
C_f	.0639	.0558	.0853	.0660	.0594	.0760
RE	1503	1693	1116	1373	1486	1236

TABLE XXII.

Data for Concentric Annular Duct, Laminar Flow
Data Set 2

Run Number

	1	2	3	4	5	6
P_1 - in. Hg	20.64	22.39	25.13	28.38	30.41	31.40
P_2	20.16	21.85	24.53	27.65	29.65	30.65
P_3	19.50	21.16	23.74	26.79	28.65	29.68
P_4	13.88	15.10	16.83	19.00	20.30	21.08
P_5	8.18	8.48	9.44	10.64	11.75	12.30
P_6	2.87	3.06	3.40	3.80	4.04	4.18
Temp - F	88.0	88.2	88.7	89.2	89.8	88.0
$\dot{m}$ - lbm/sec	1.56	1.70	1.92	2.14	2.31	2.28
V - ft/sec	7.52	8.19	9.25	10.3	11.1	11.0
λ	.0842	.0775	.0677	.0616	.0569	.0605
RE	1071	1170	1332	1500	1627	1565

TABLE XXIII.

Data for Concentric Annular Duct, Transition Flow
Data Set 1

<u>Run Number</u>

	1	2	3	4	5
P_1 - in. Hg	34.10	33.30	31.35	30.02	28.85
P_2	33.16	32.40	30.45	29.20	28.10
P_3	31.96	31.25	29.38	28.18	27.05
P_4	23.15	22.50	21.24	20.30	19.50
P_5	13.08	12.56	12.22	11.70	11.28
P_6	4.49	4.38	4.15	3.99	3.85
Temp - F	90.0	90.2	92.0	93.0	94.0
$\dot{m}$ - lbm/sec	2.54	2.49	2.42	2.37	2.33
V - ft/sec	12.2	12.0	11.7	10.8	11.2
C_f	.0538	.0543	.0544	.0606	.0536
RE	1801	1770	1758	1645	1736

64

TABLE XXIV.

Data for Concentric Annular Duct, Transition Flow
Data Set 2

Run Number

	1	2	3	4	5
P_1 - in. Hg	27.95	24.96	34.00	33.20	35.00
P_2	27.20	24.30	33.06	32.30	34.05
P_3	26.28	23.51	31.96	31.30	33.00
P_4	18.20	16.66	22.73	22.20	23.42
P_5	10.70	9.46	13.05	12.90	13.43
P_6	3.70	3.35	4.46	4.40	4.60
Temp - F	95.0	96.5	90.0	88.3	89.5
$\dot{m}$ - lbm/sec	2.20	2.08	2.55	2.43	2.60
V - ft/sec	10.6	10.0	12.3	11.7	12.5
C_f	.0557	.0572	.0523	.0565	.0518
RE	1660	1649	1808	1676	1828

Appendix D

Viscosity Comparison

This appendix compares viscosity calculated using the Hagen-Poiseuille Law verses extrapolated values from Table VI. The Hagen-Poiseuille Law is used with circular duct flow data at various temperatures. Table VI values are extrapolated from two data points using a Viscosity-Temperature chart.

TABLE XXV.

Viscosity Comparison

Re	dP/dx in.Hg/ft	V ft/sec	μ - H-P calcs lbf-sec/ft^2	μ - Table VI lbf-sec/ft^2
1132	.0625	2.527	2.500×10^{-4}	2.420×10^{-4}
1426	.0770	3.162	2.470	2.510
1574	.0700	3.146	2.254	2.264
1636	.1000	3.817	2.654	2.642
1698	.0700	3.352	2.120	2.240

Since the extrapolated values from Table VI predict those calculated, using the Hagen-Poiseuille Law, they will be used in all other calculations, for the sake of convenience.

Appendix E.

Hydrodynamic Entrance Length Plots
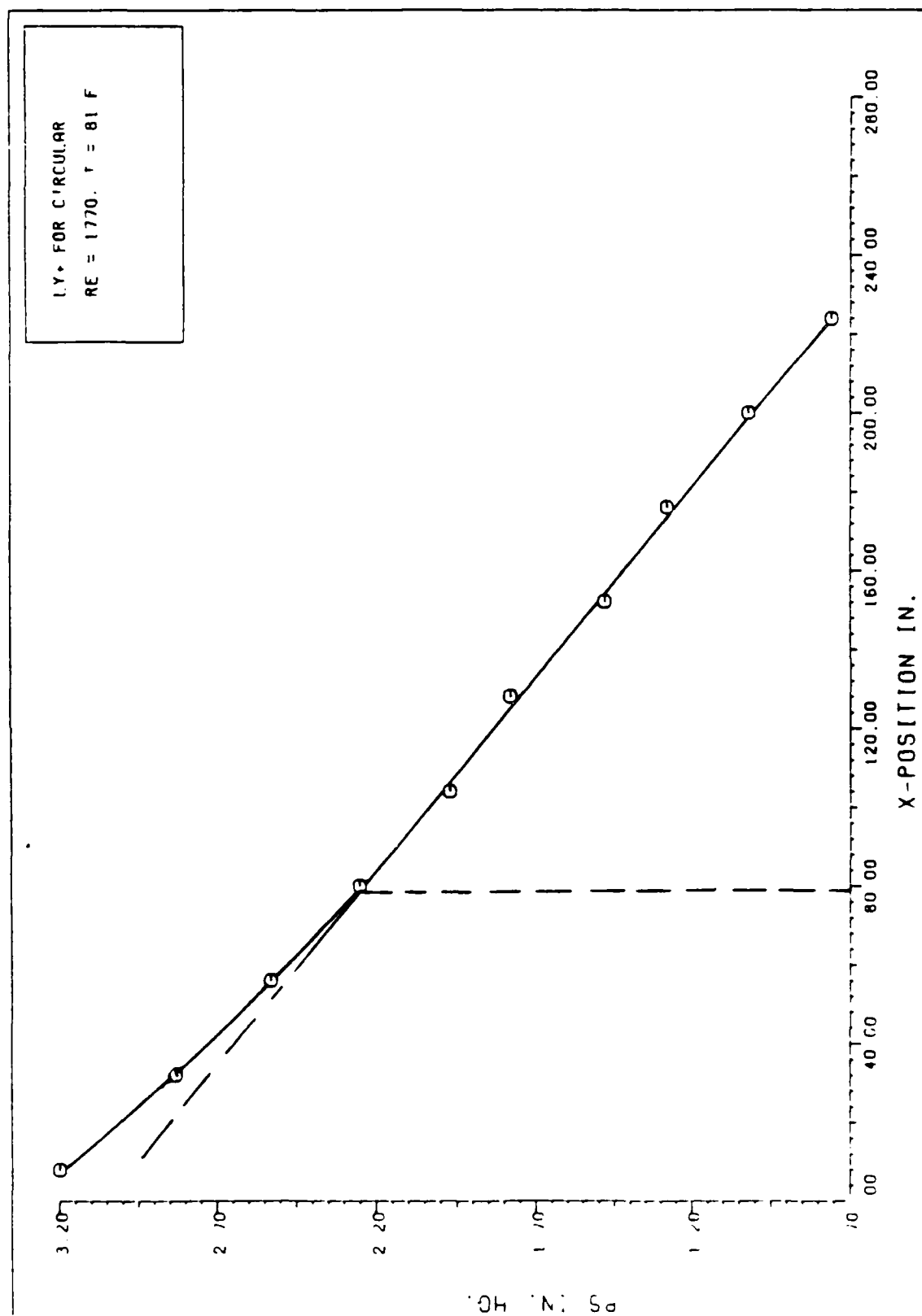
Figure 20. Hydrodynamic Entrance Length for Circular Duct, Re = 1770.
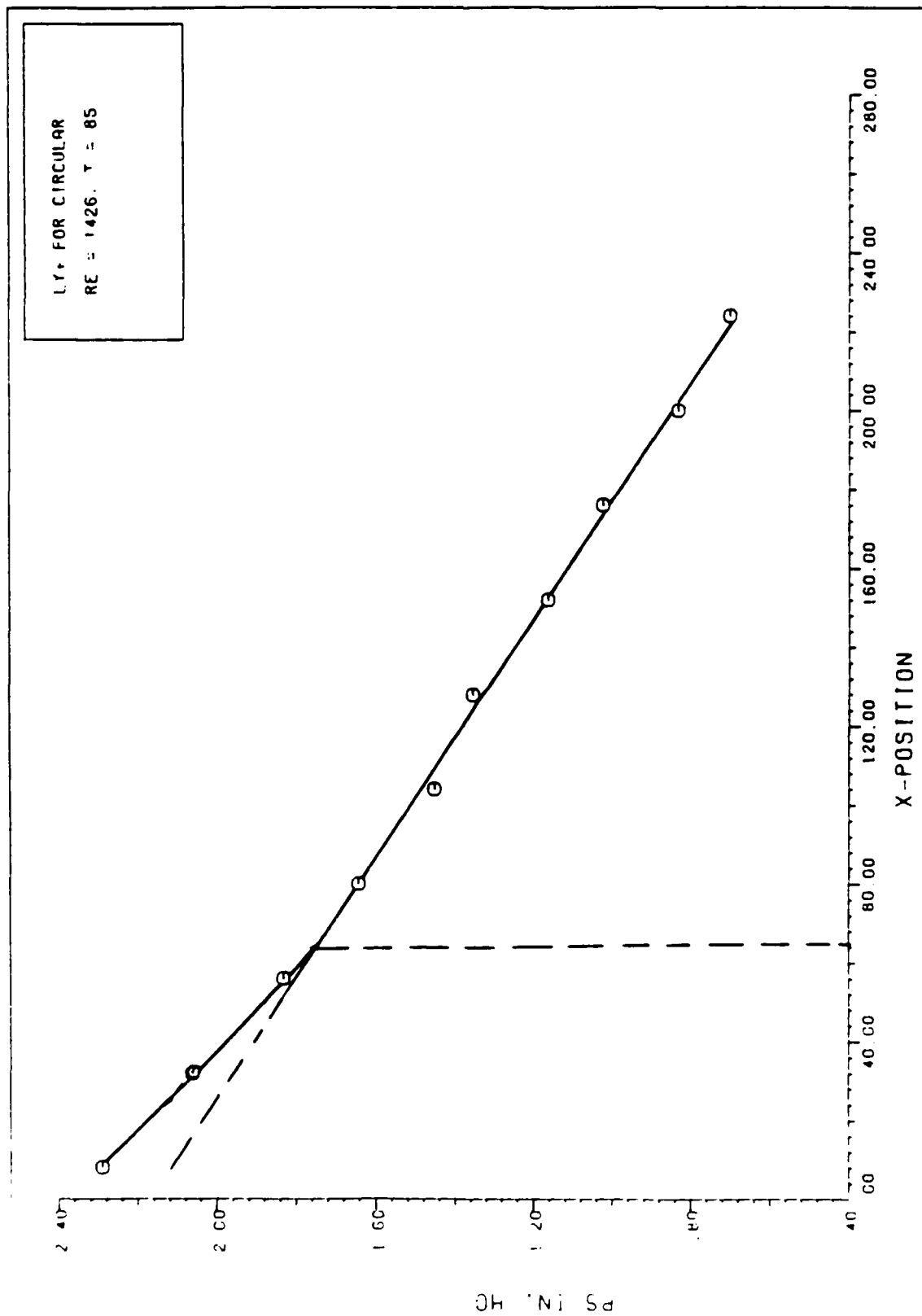
Figure 21. Hydrodynamic Entrance Length for Circular Duct, Re = 1426.

69
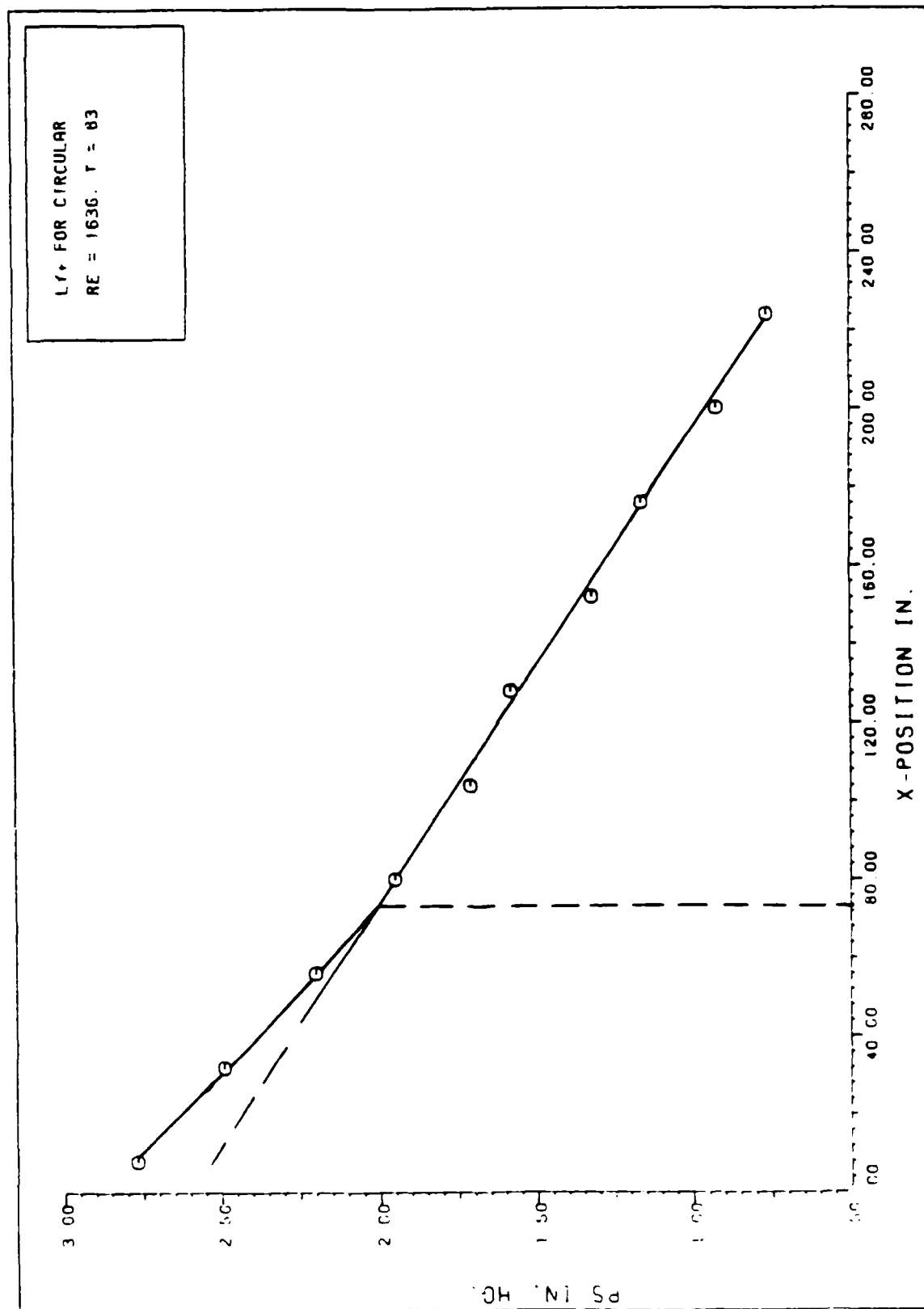
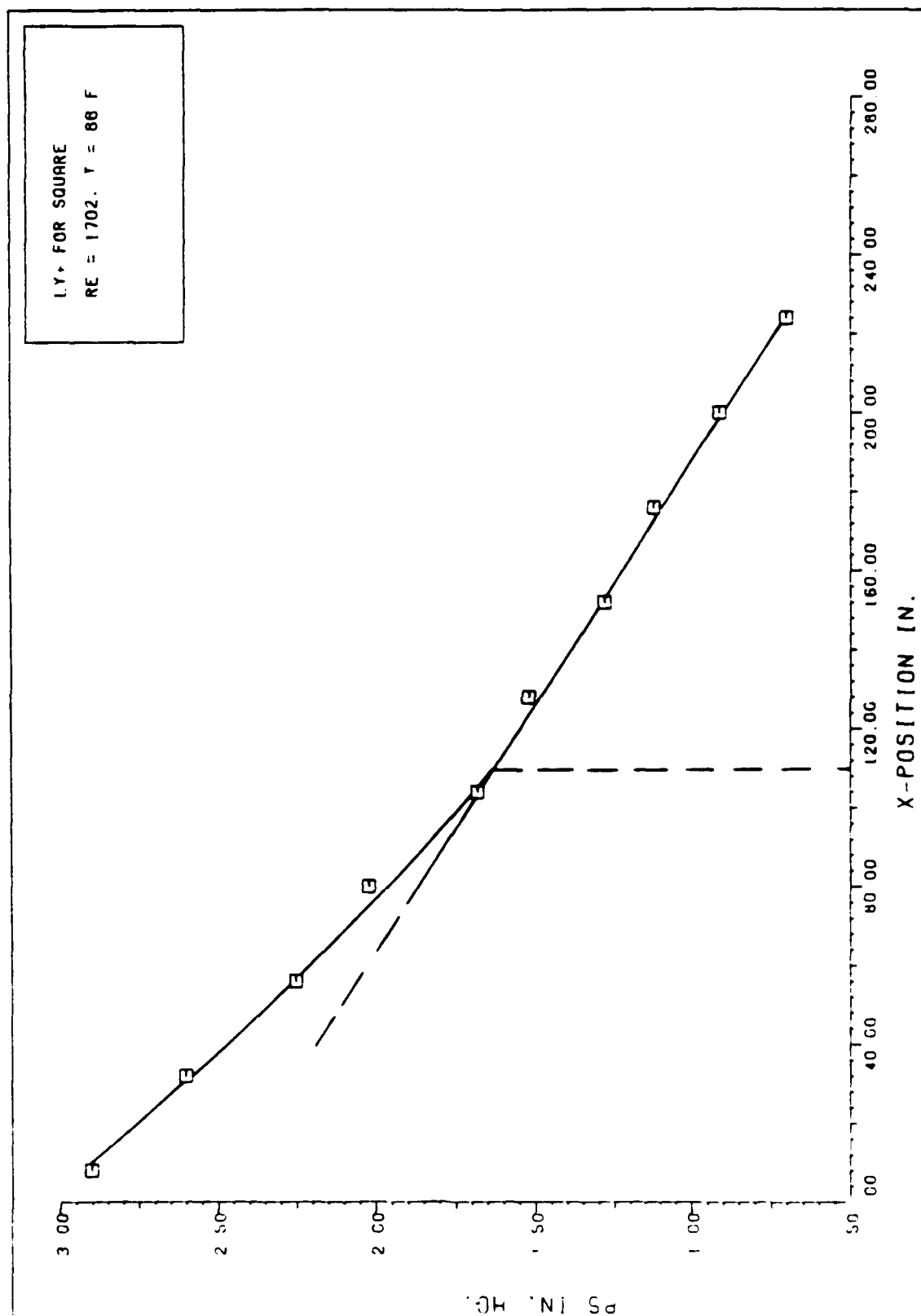Figure 22. Hydrodynamic Entrance Length for Circular Duct, Re = 1636.
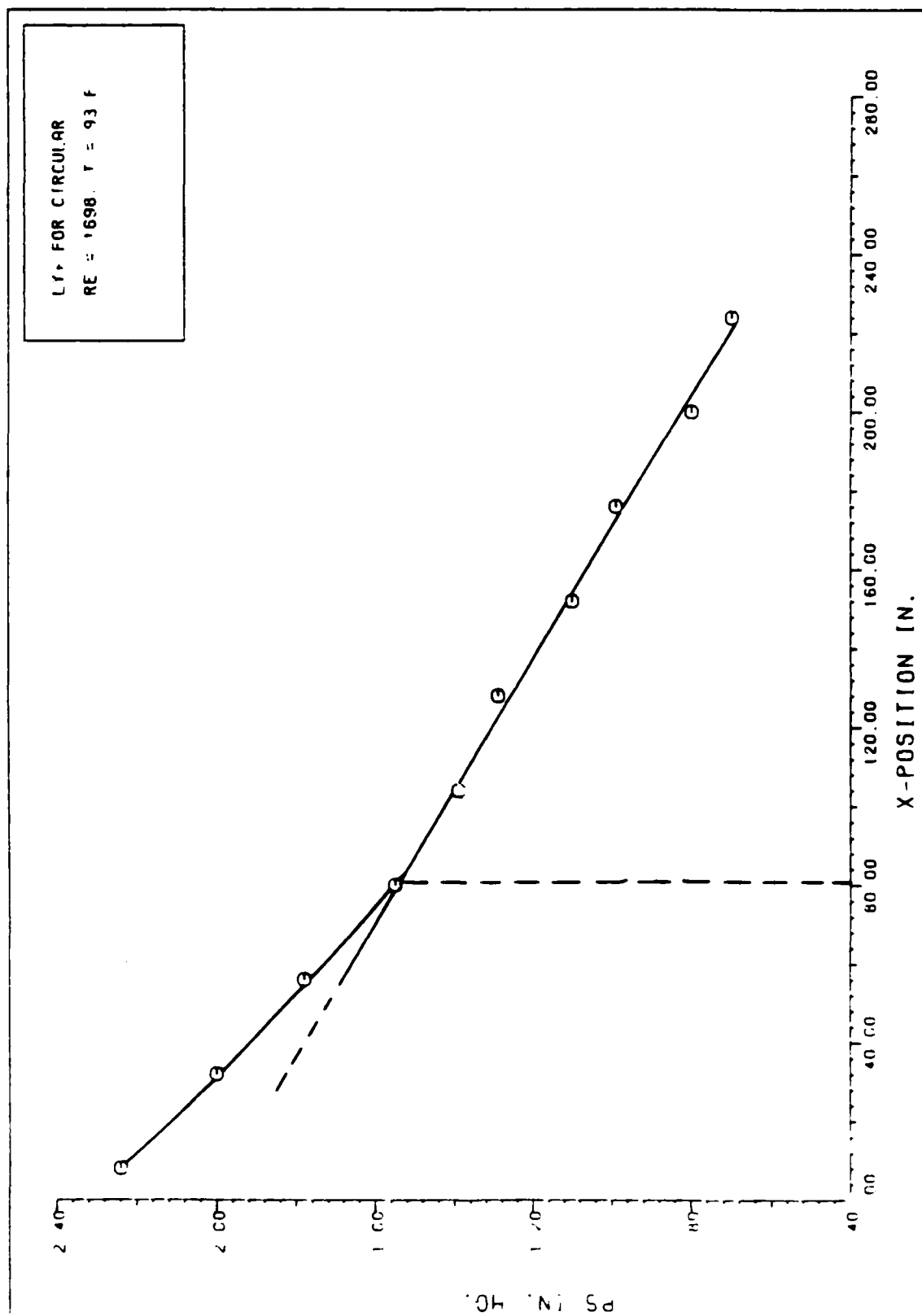
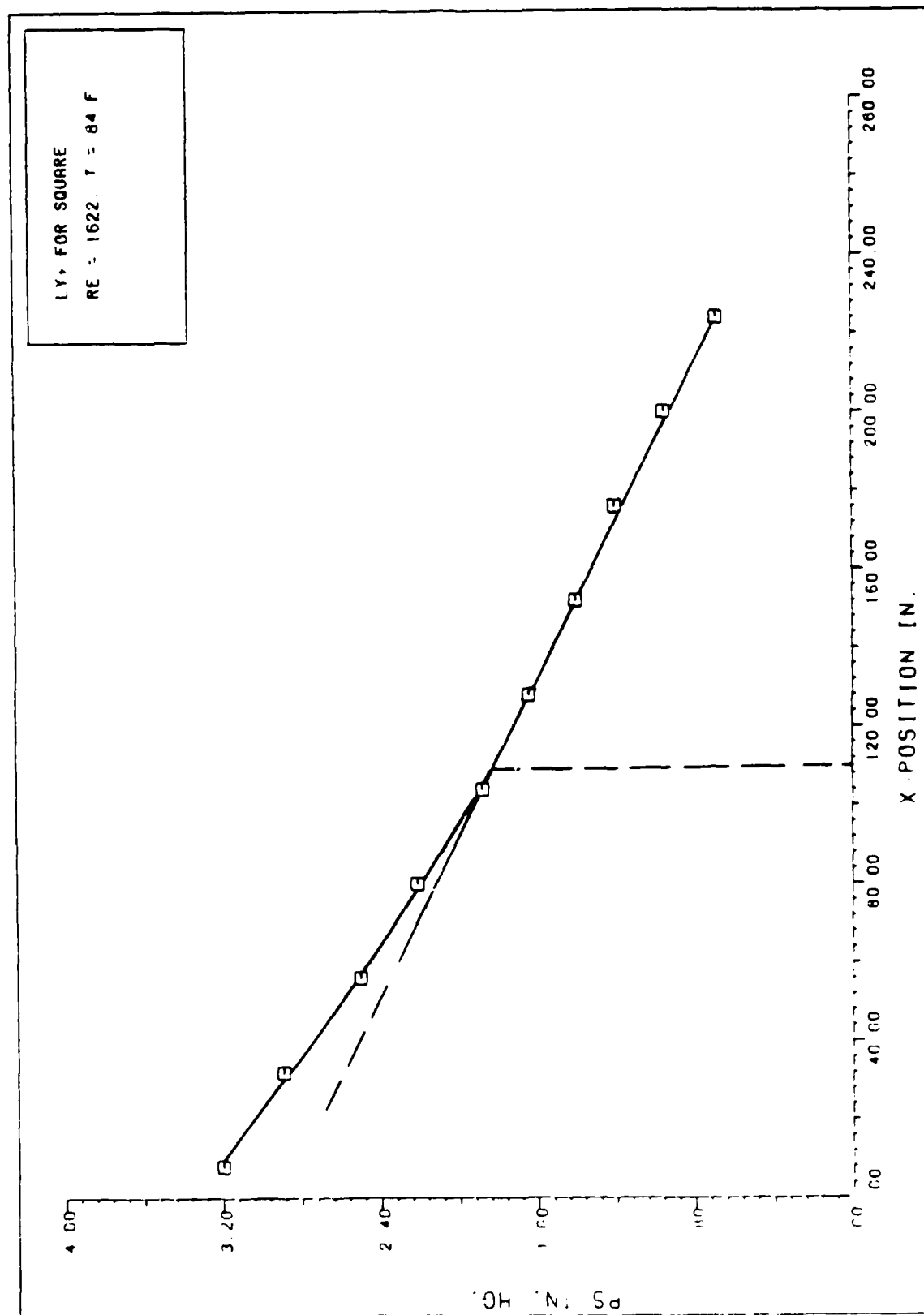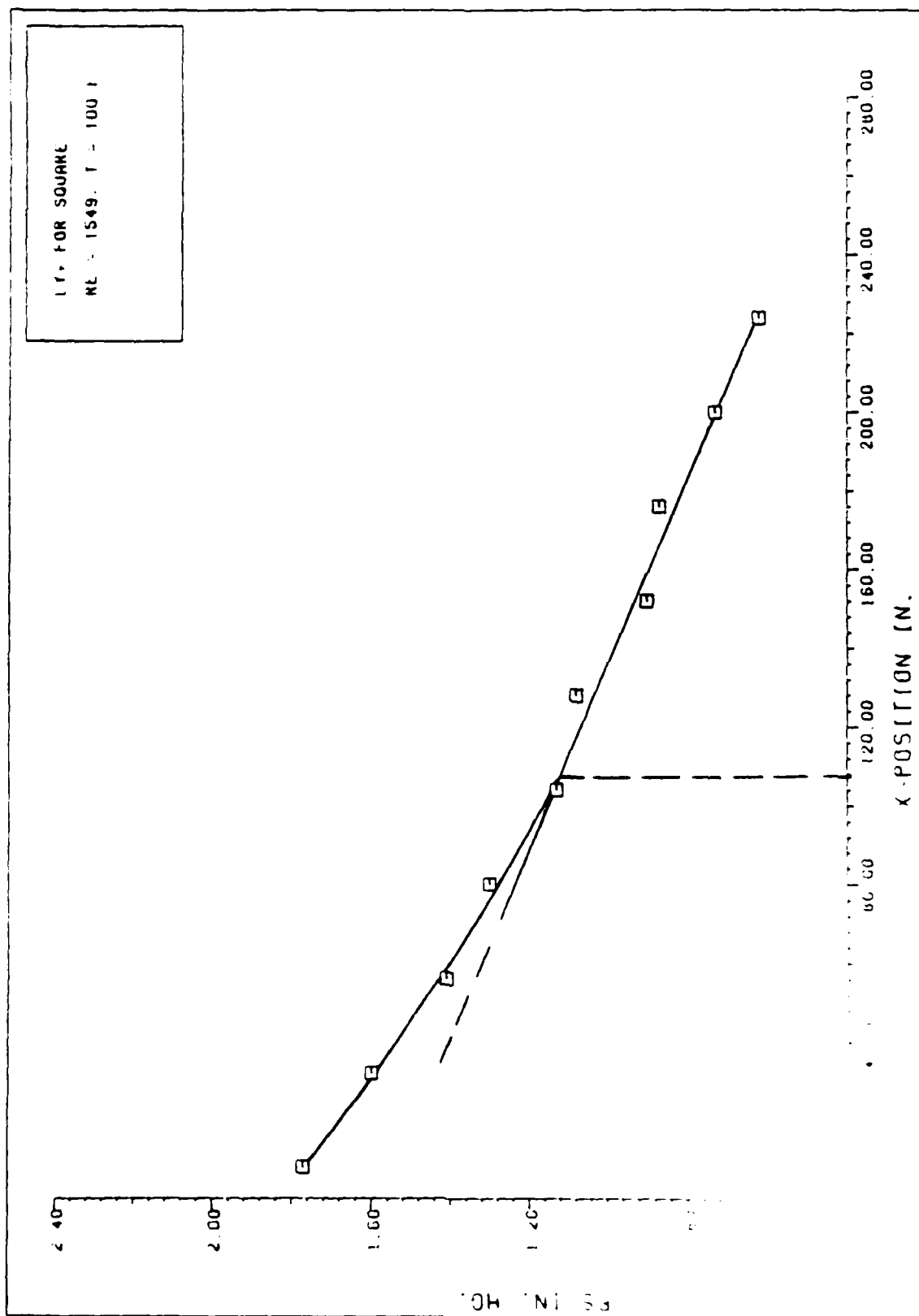Figure 23. Hydrodynamic Entrance Length for Circular Duct, Re = 1698.
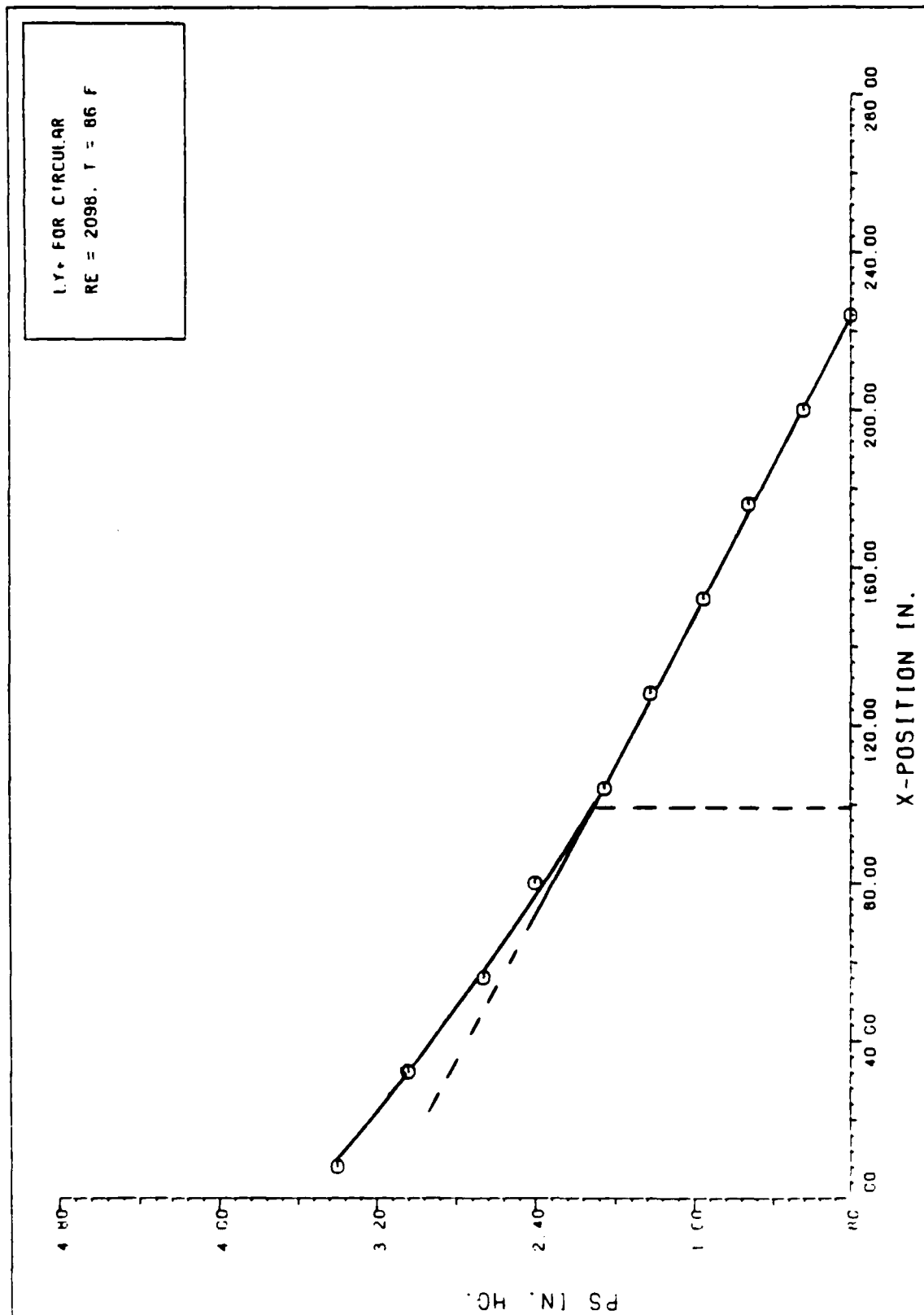
Figure 24. Hydrodynamic Entrance Length for Circular Duct, Re = 2098.

72
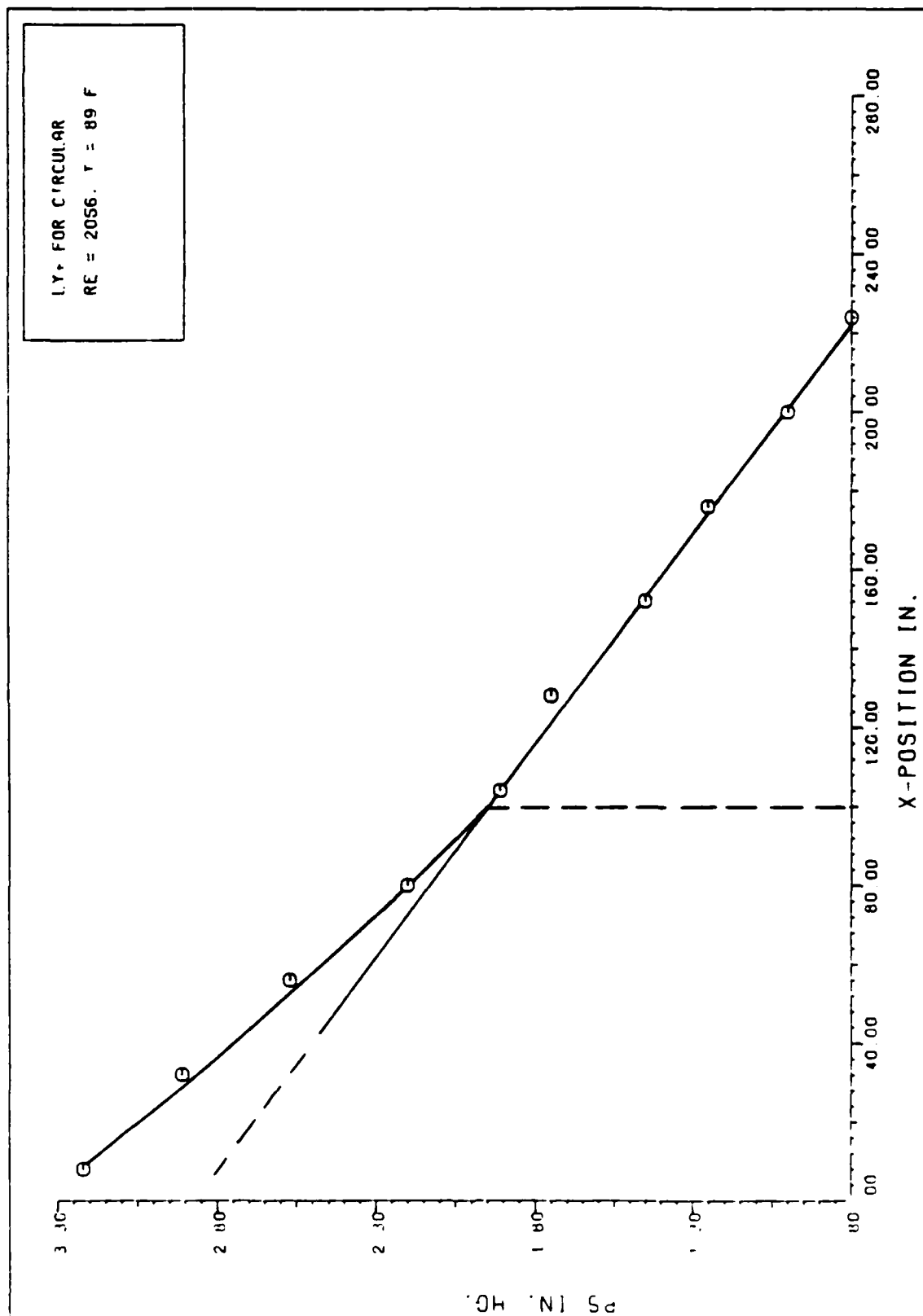
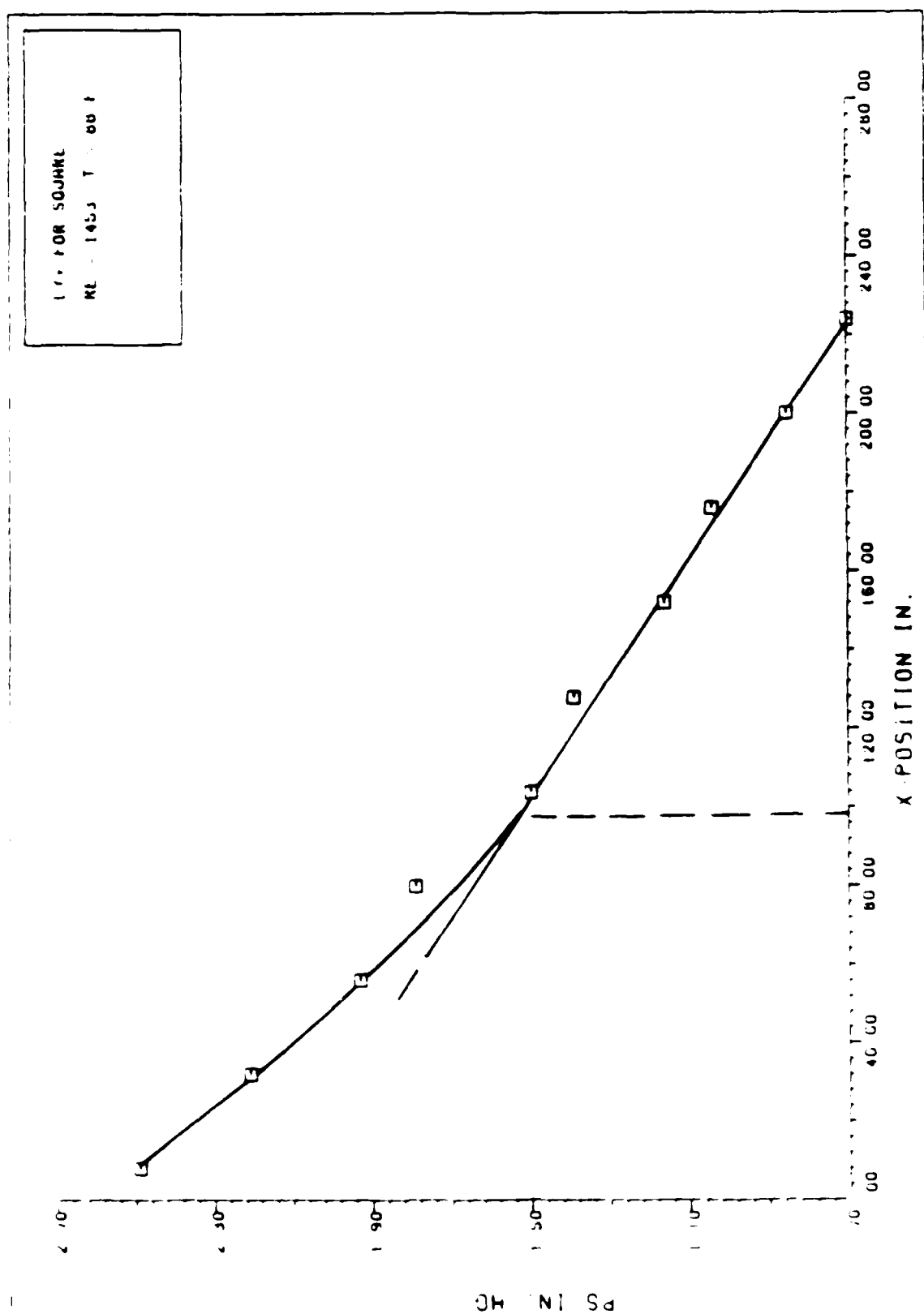Figure 25. Hydrodynamic Entrance Length for Circular Duct, Re = 2056.
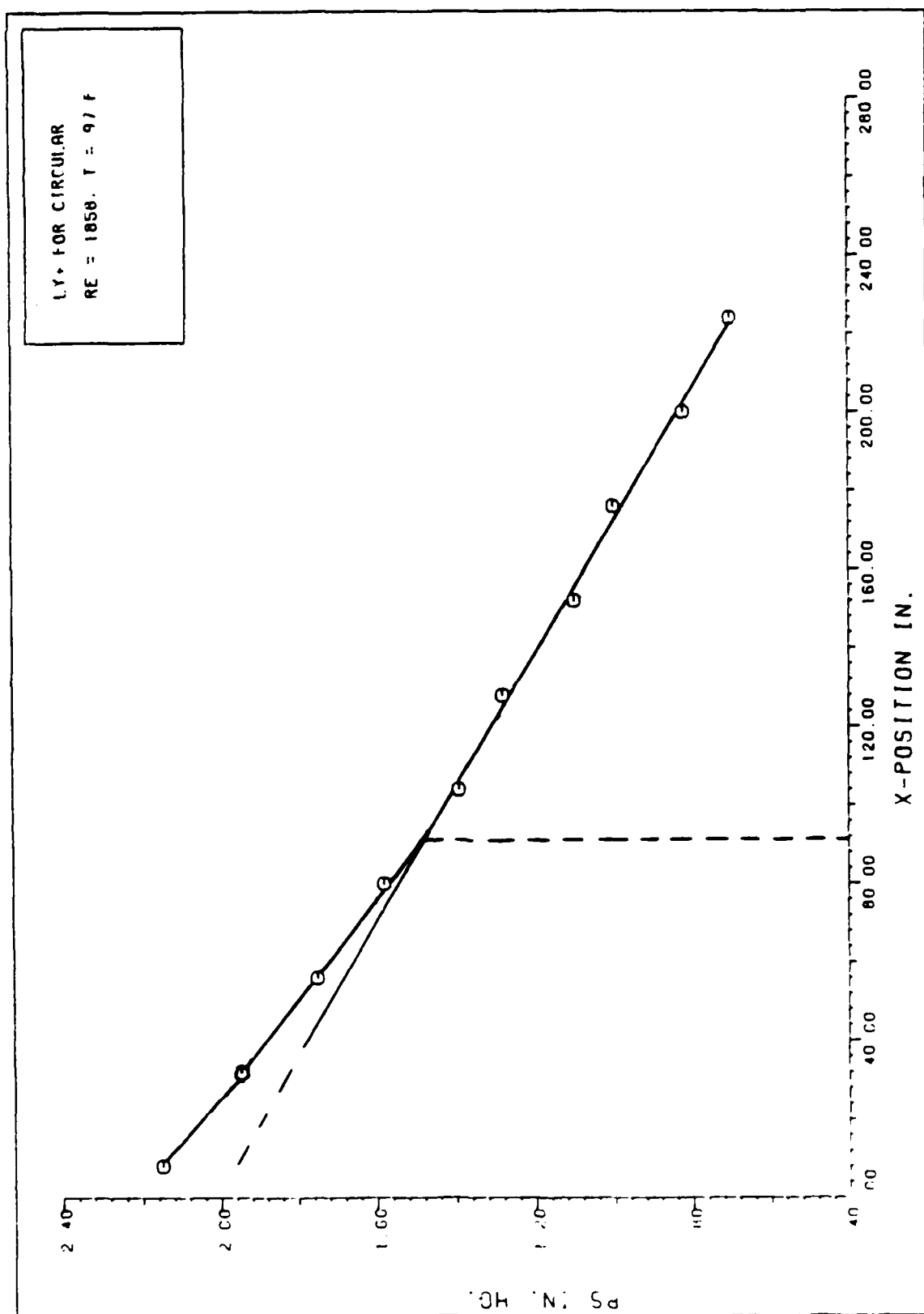
Figure 26. Hydrodynamic Entrance Length for Circular Duct, Re = 1858.
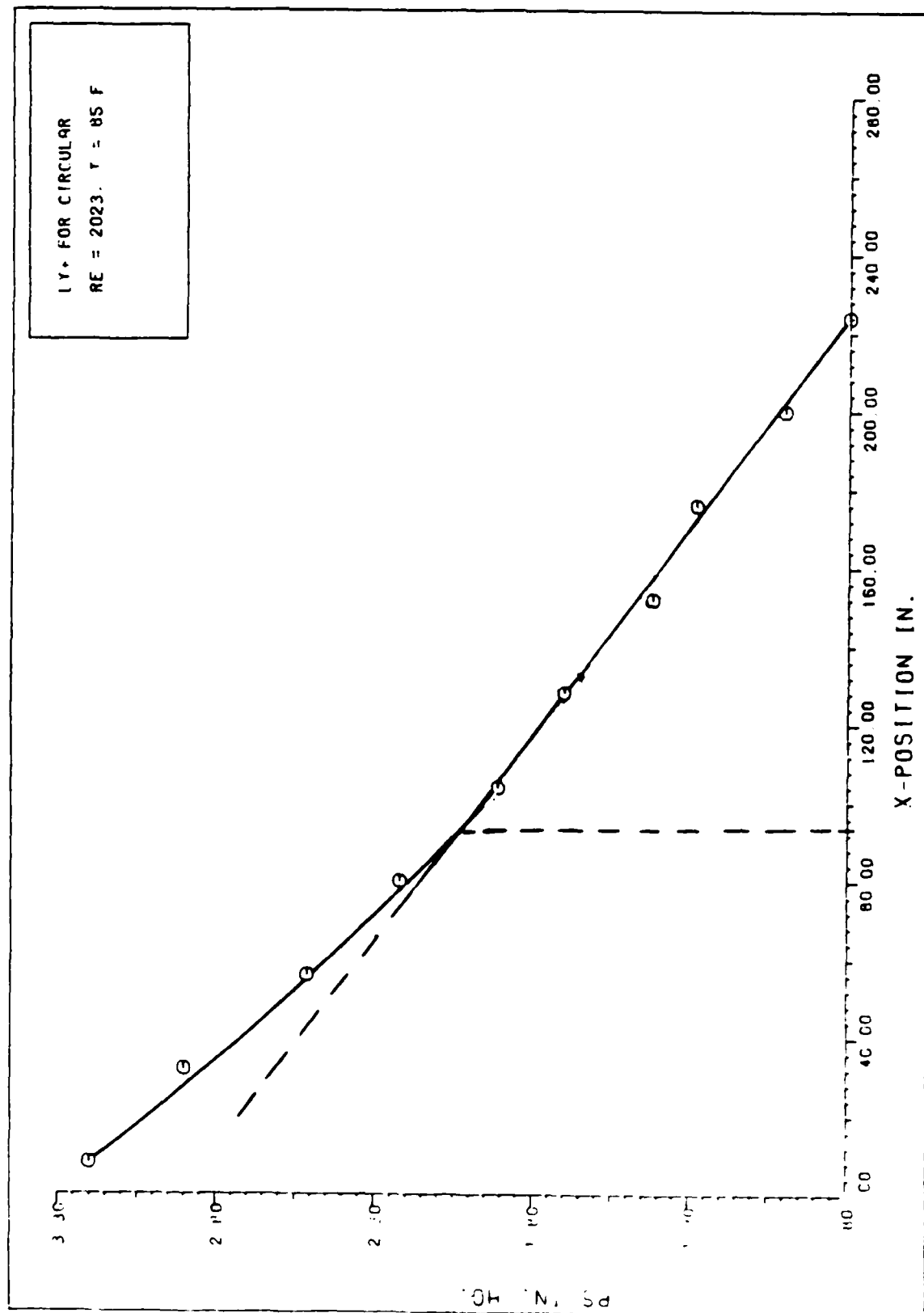
Figure 27. Hydrodynamic Entrance Length for Circular Duct, Re = 2023.
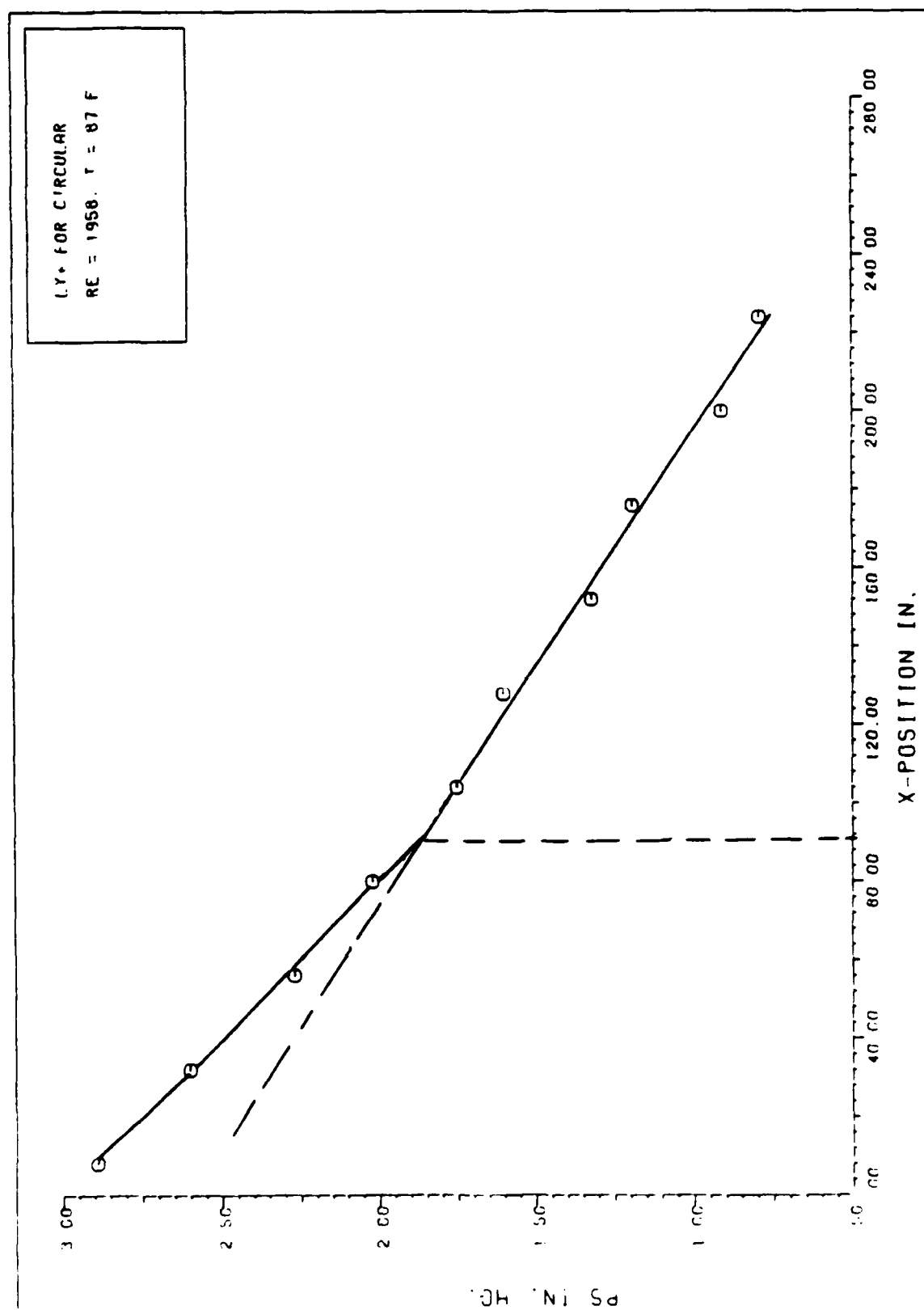
Figure 28. Hydrodynamic Entrance Length for Circular Duct, Re = 1958.

Figure 29. Hydrodynamic Entrance Length for Circular Duct, Re = 2014.

77

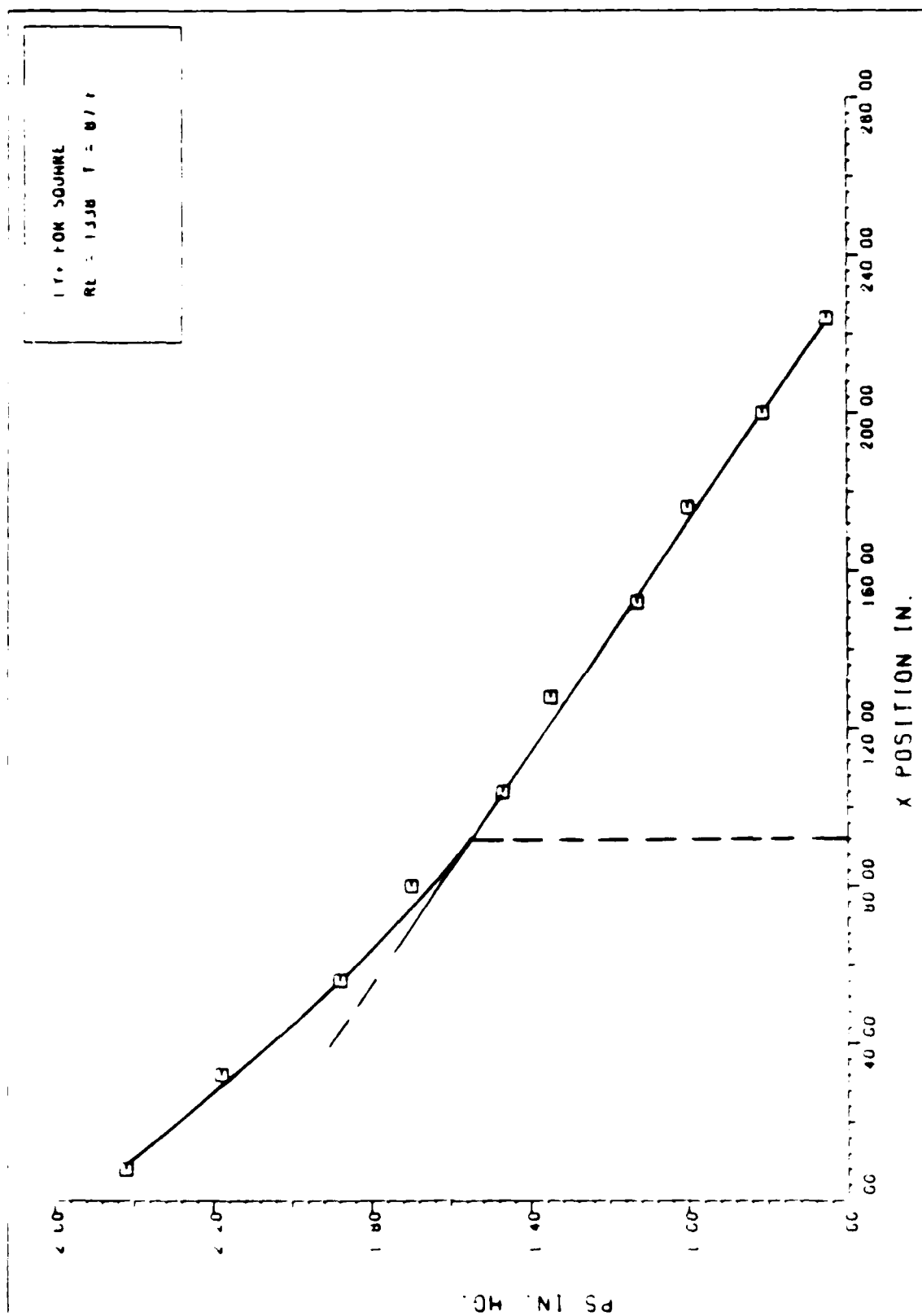Figure 30. Hydrodynamic Entrance Length for Square Duct, Re = 1410.

Figure 32. Hydrodynamic Entrance Length for Square Duct, Re = 1691.

80

Figure 31. Hydrodynamic Entrance Length for Square Duct, Re = 1702.

Figure 33. Hydrodynamic Entrance Length for Square Duct, Re = 1622.
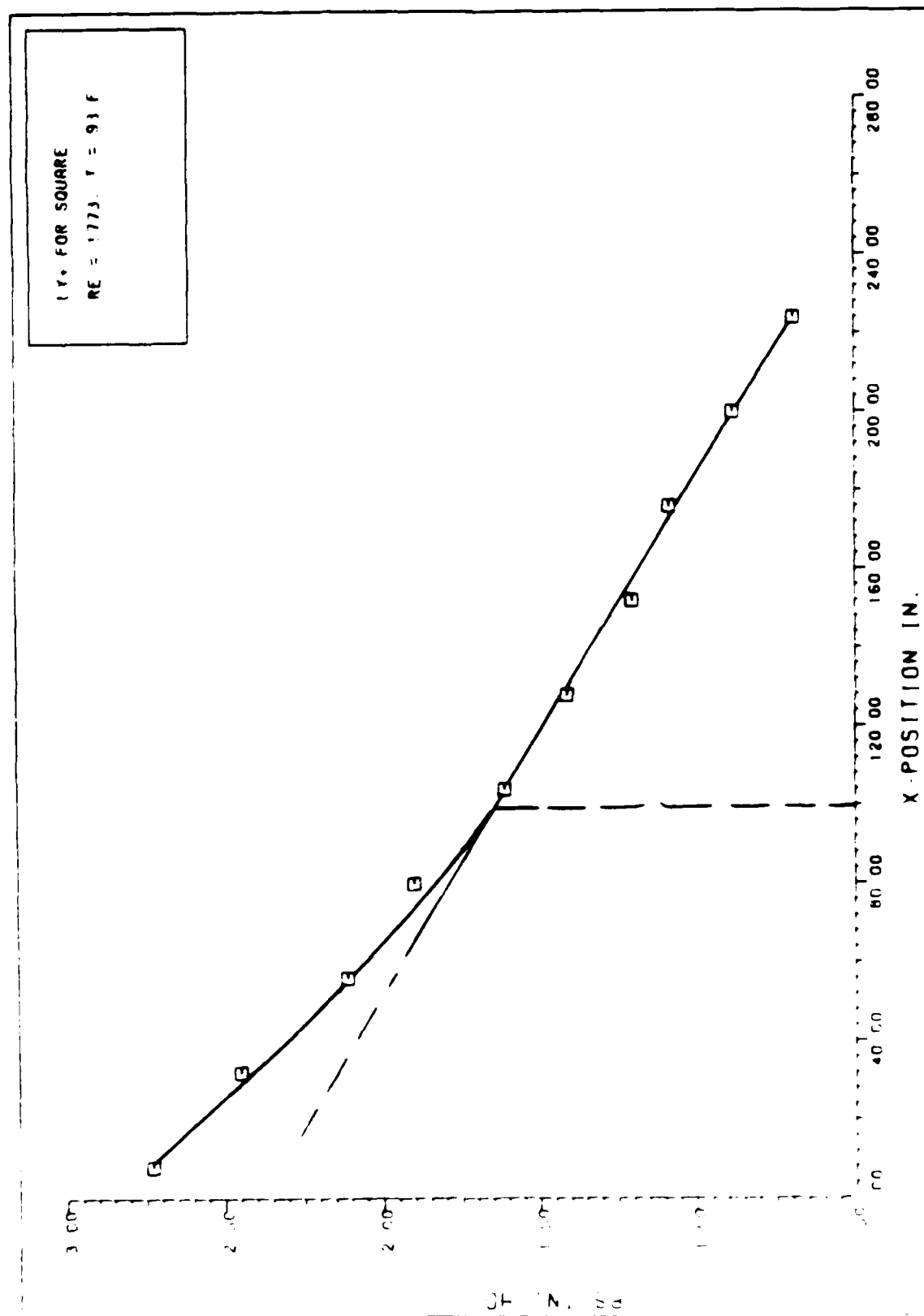
... ratation Length for Square Duct, Re = 1549.

Figure 3. Wall distance, length for square duct, Re = 1500.

POSITION IN X

POSITION IN

Figure 36. Hydrodynamic Entrance Length for Square Duct, Re = 1453.

Figure 3'. Hydrodynamic Entrance Length for Square Duct, Re = 1338.

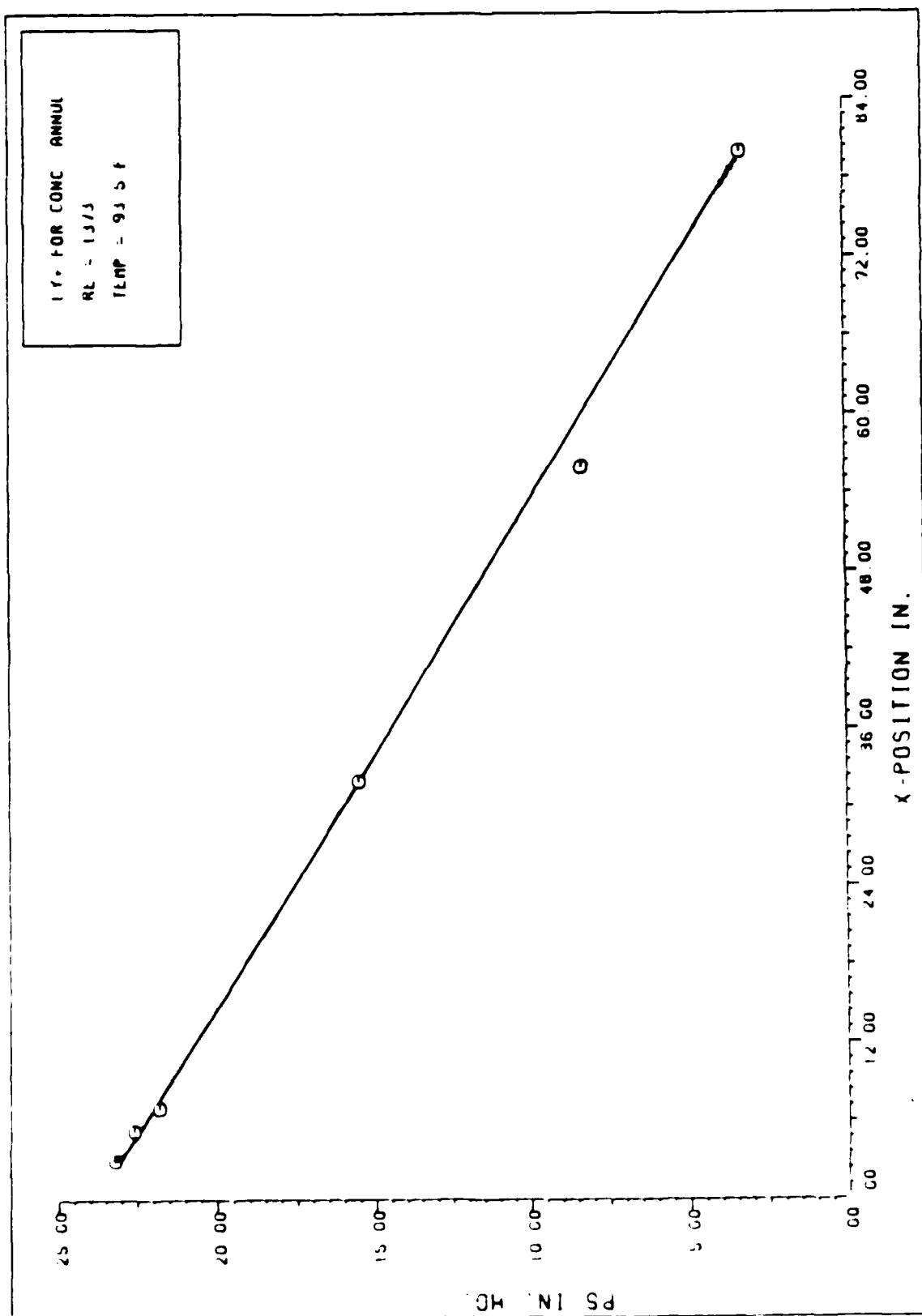Figure 36. Hydrodynamic Entrance Length for Square Duct, Re = 1773.

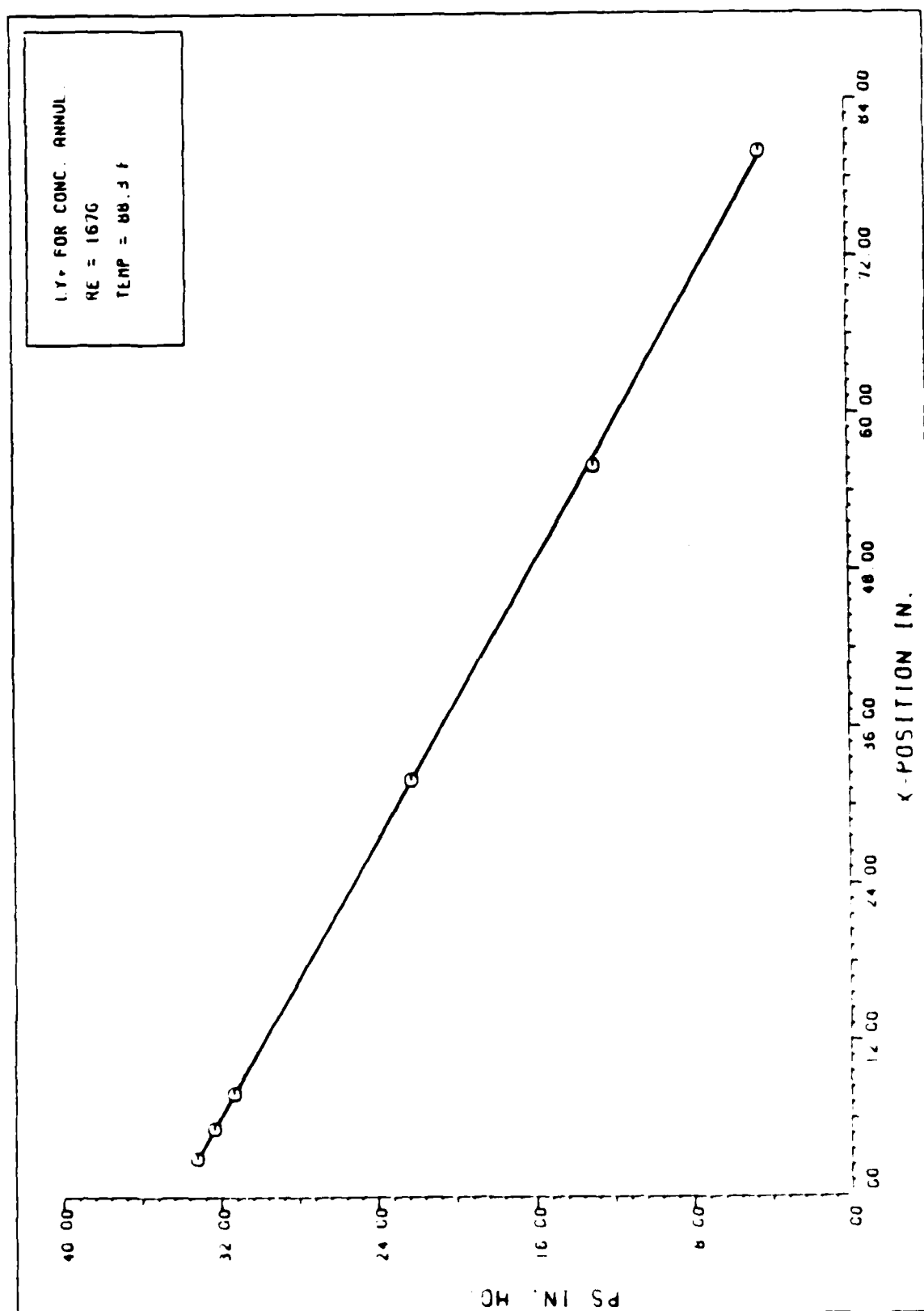Figure 39. Hydrodynamic Entrance Length for Concentric Annular Duct, Re = 1373.

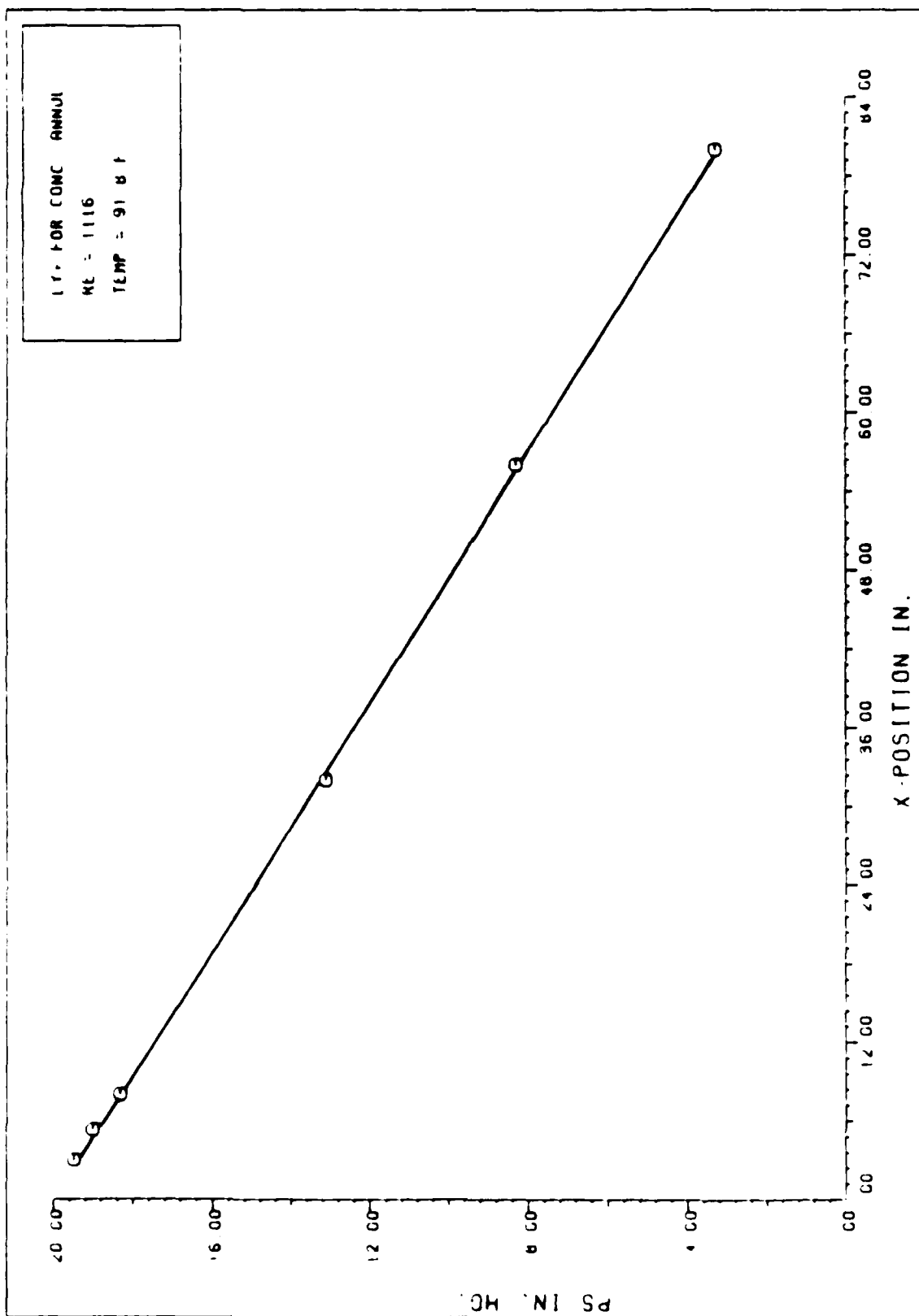Figure 20. Hydrodynamic Entrance Length for Concentric Annular Duct, Re = 1676.

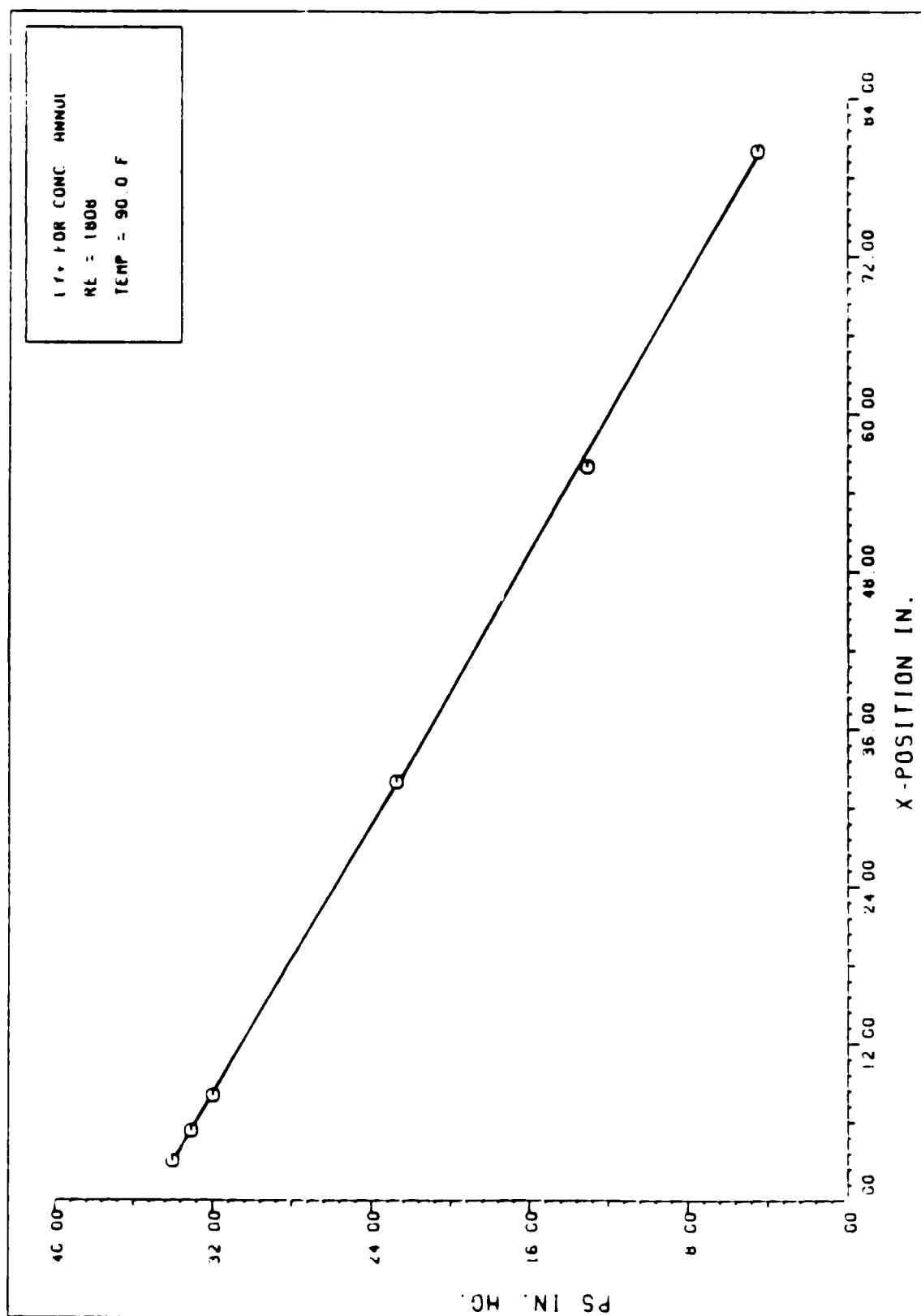Figure 41. Hydrodynamic Entrance Length for Concentric Annular Duct, Re = 1116.

Figure 42. Hydrodynamic Entrance Length for Concentric Annular Duct, Re = 1808.

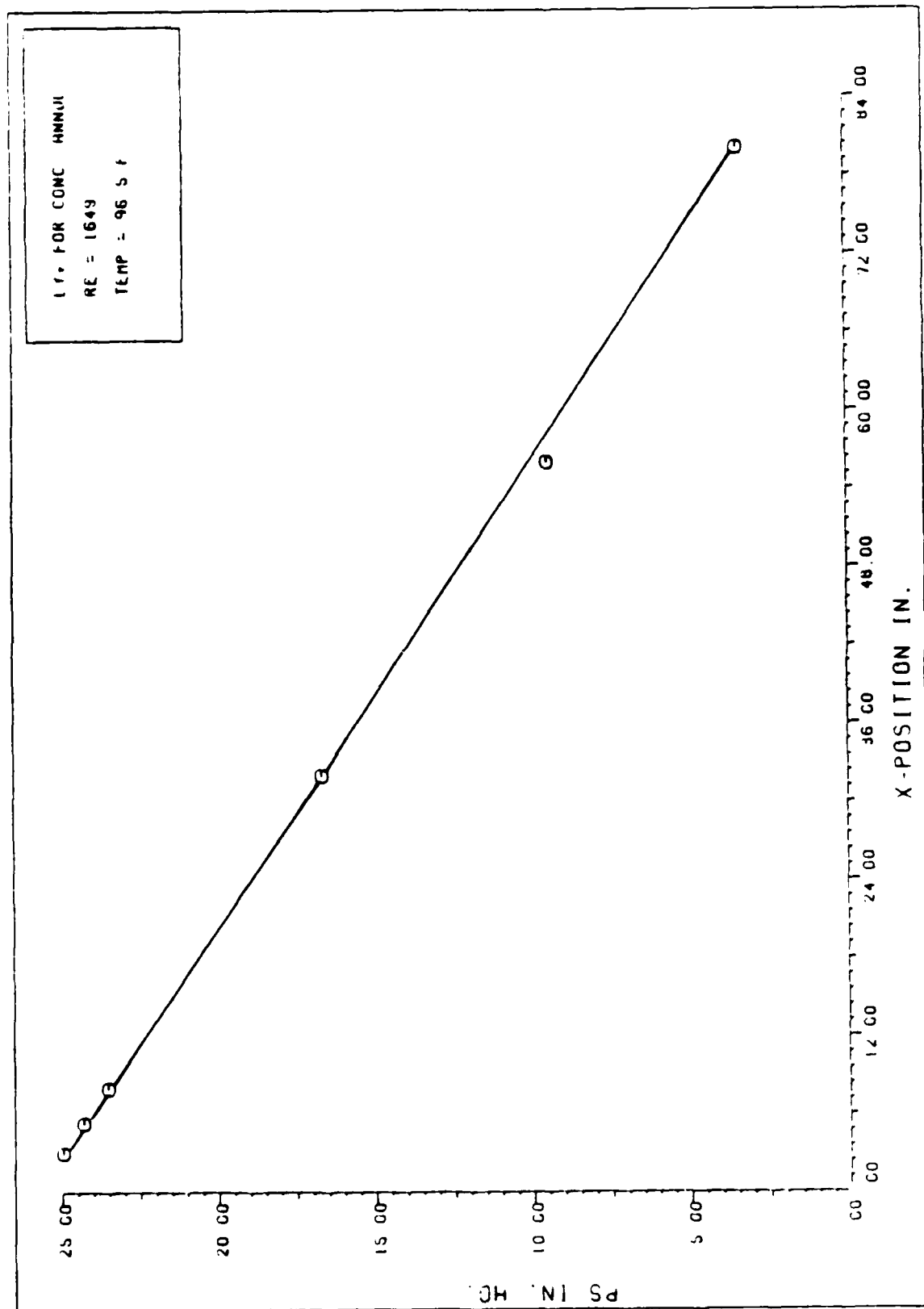Figure 43. Hydrodynamic Entrance Length for Concentric Annular Duct, Re = 1649.

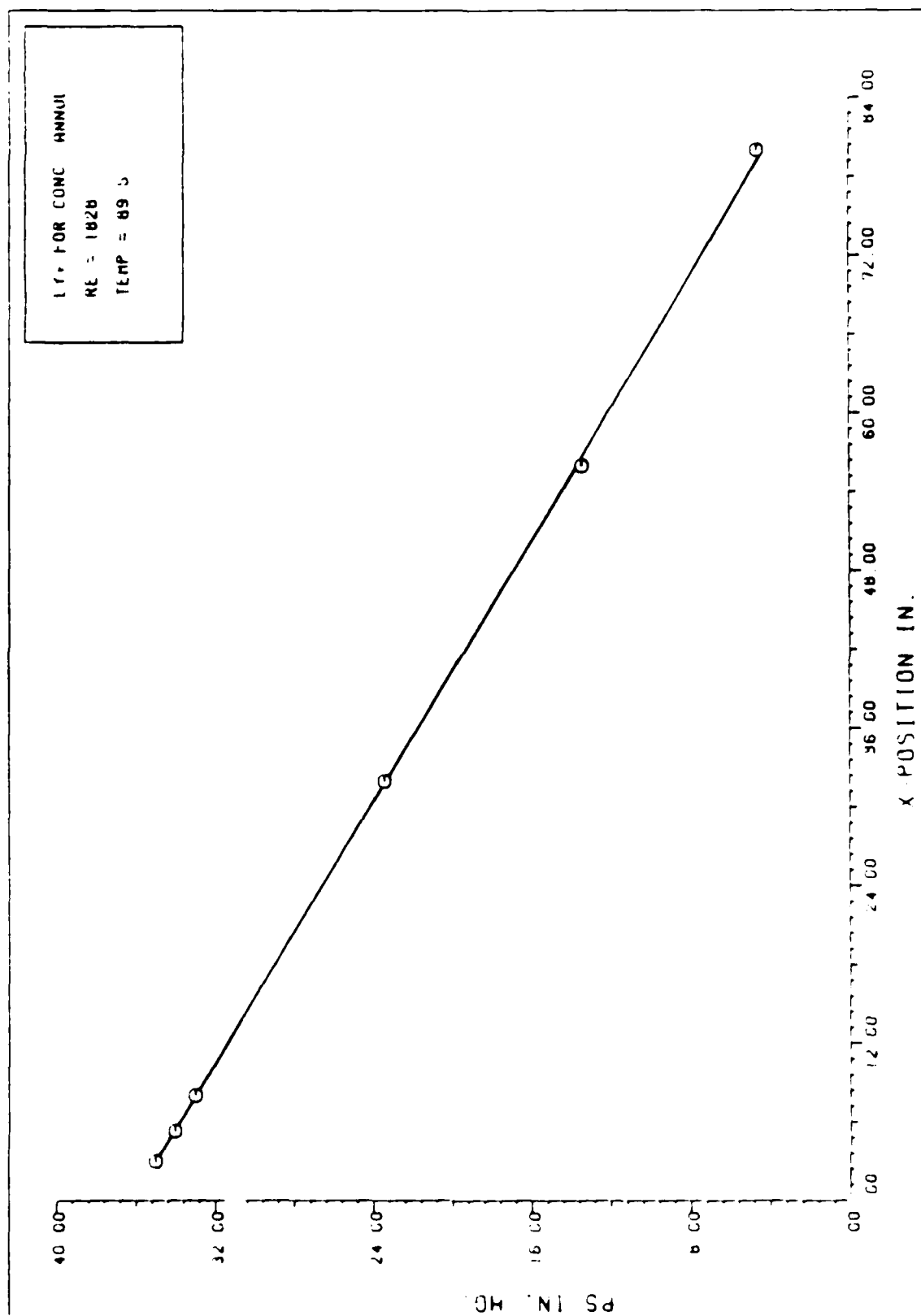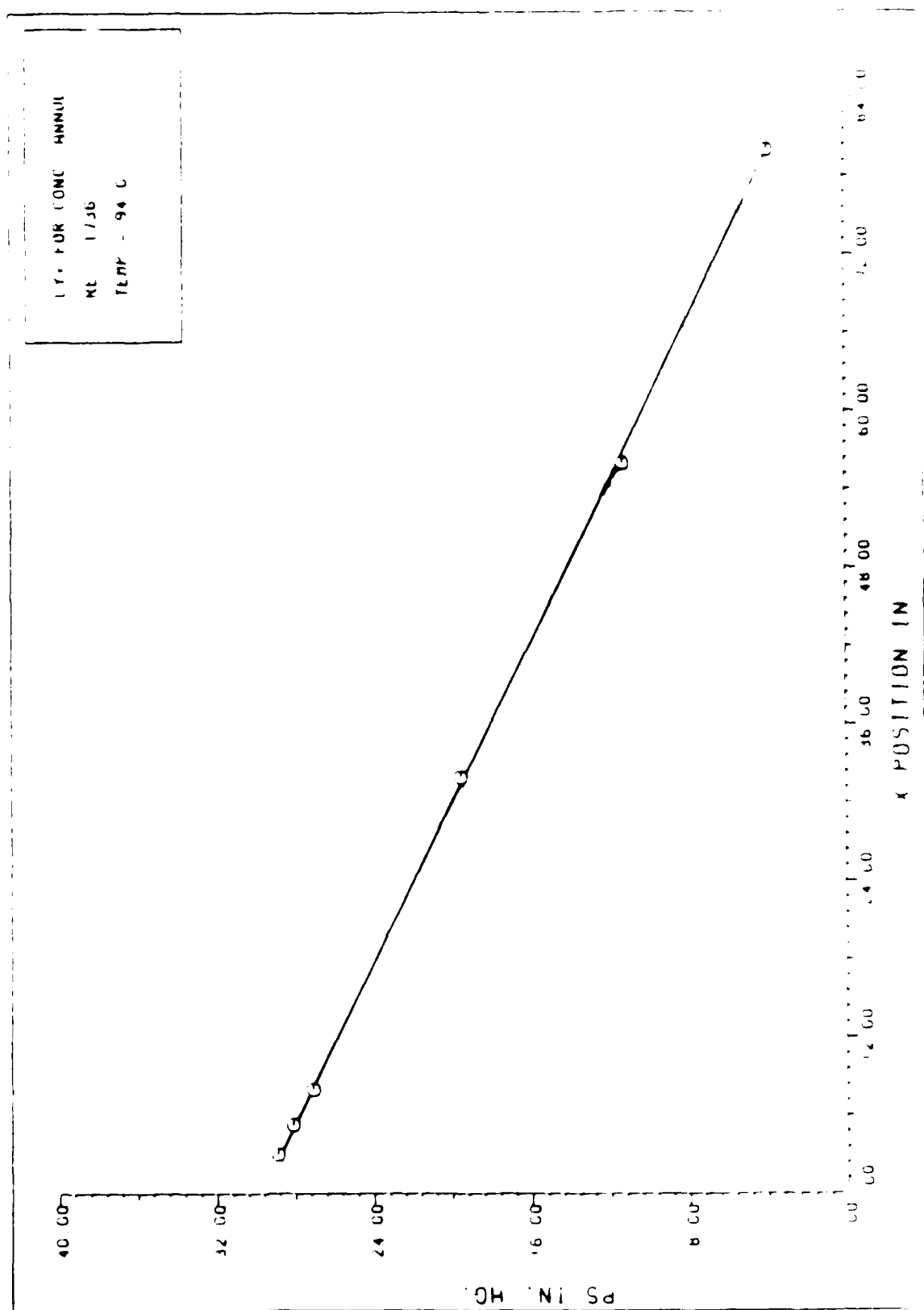Figure 44. Hydrodynamic Entrance Length for Concentric Annular Duct, Re = 1828.

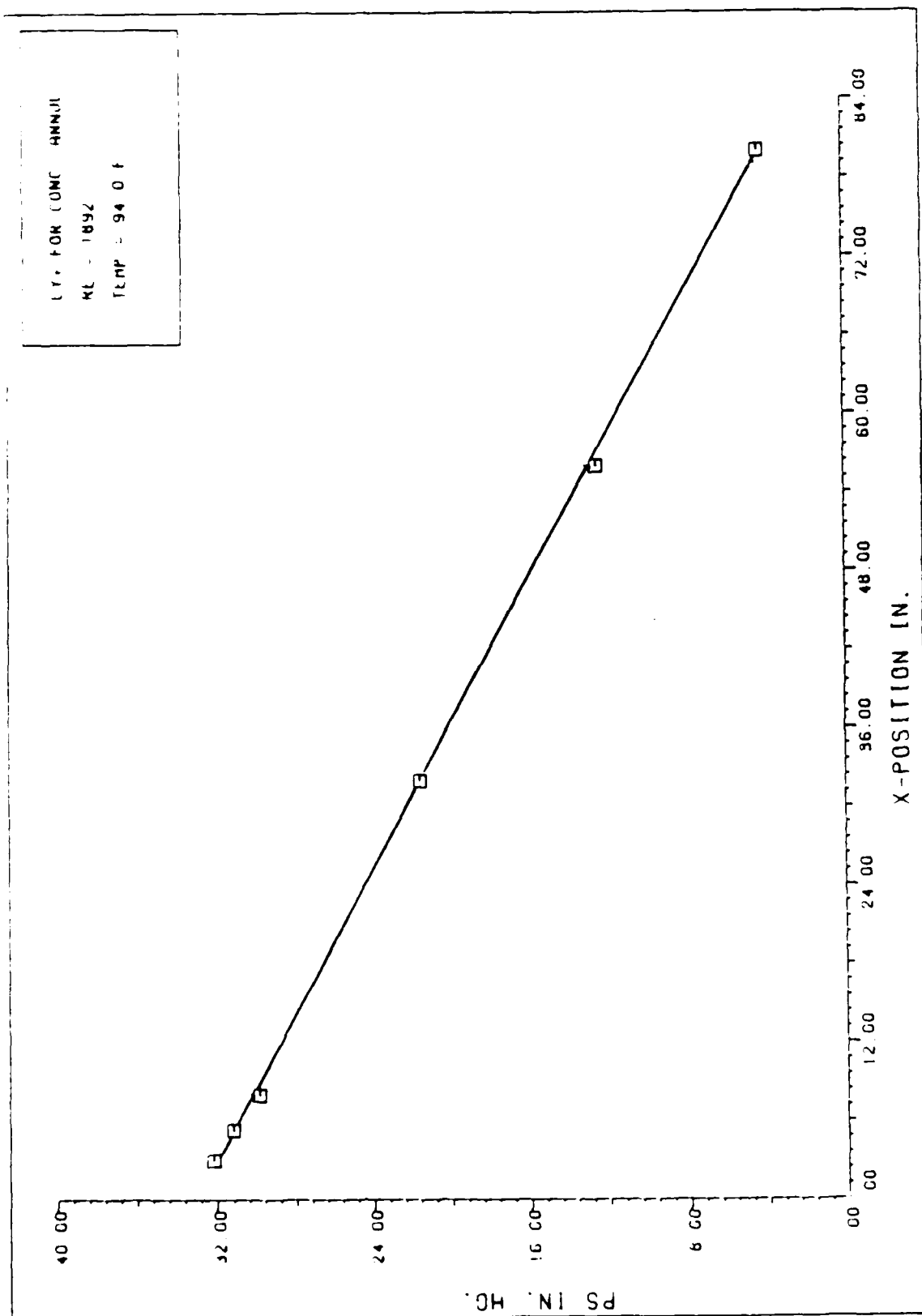Figure ... High Velocity Entrance Length for Concentric Annular Duct, Re 1 sec.

Figure 46. Hydrodynamic Entrance Length for Concentric Annular Duct, Re = 1892.

Bibliography

1. Kays, William M. and Michael E. Crawford. <u>Convective Heat and Mass Transfer</u>(Second Edition). New York: McGraw-Hill Book Company, 1980.

2. Schlichting, H. <u>Boundary Layer Theory</u>(Fourth Edition). New York: McGraw-Hill Book Company, 1960.

3. Shah, R. K. and A. L. London. <u>Laminar Flow Forced Convection in Ducts</u>. Supplement 1 to Advances in Heat Transfer. New York: Academic Press, 1978.

4. Shapiro, A. H. <u>The Dynamics and Thermodynamics of Compressible Fluid Flow, Volume 1</u>. New York: Ronald Press Company, 1953.

5. Bejan, A. <u>Convective Heat Transfer</u>. New York: Wiley and Sons, 1984.

6. Stanton, T. E. and J. R. Pannel. "Similarity of Motion in Relation of the Surface Friction of Fluids," <u>Phil. Trans. Roy. Soc.</u>, <u>A 214</u>: 199 (1914).

7. Senecal, V. E. and R. R. Rothfus. "Transition Flow of Fluids in Smooth Tubes," <u>Chemical Engineering Progress</u>, <u>49</u>: 533 (1953).

8. Shiller, L. "Uber den Stromungswiderstand Von Rohren Verschiedenen Querschnitts und Ranhigkeitsgrades," <u>ZAMM</u>, <u>3</u>: 2-13 (1923).

9. Nikuradse, J. "Turbulente Stromung in Nicht Kreisformigen Rohren," <u>Ing. Arch.</u>, <u>1</u>: 306-332 (1930).

10. Koch, R. and F. Feind. "Druckverlust und Warmeubergang in Ringspulten," <u>Chemie-Ing-Techn.</u>, <u>30</u>: 577-584 (1958).

11. Burmeister, L. C. <u>Convective Heat Transfer</u>. New York: Wiley and Sons, 1983.

12. Vennard, J. K. <u>Elementary Fluid Mechanics</u>. New York: Wiley and Sons, 1961.

13. Barna, P. S. <u>Fluid Mechanics for Engineers</u>(Second Edition). Washington D. C.: Butterworth and Company, 1964.

14. Tuve, G. L. Mechanical Engineering Experimentation. New York: McGraw-Hill Book Company, 1961.

15. Ekman, V. W. "On the Change from Steady to Turbulent Motion of Fluids," Ark. f. Mat. Astrom. och Fys., 6: No. 12 (1910).

16. Liu, J. "Flow of a Bingham Fluid in the Entrance Region of a Annular Tube," MS Thesis. University of Wisconsin-Milwaukee, 1974.

17. Heaton, H. S. et al. "Heat Transfer in Annular Passages. Simultaneous Development of Velocity and Temperature Fields in Laminar Flow," Int. Journal of Heat and Mass Transfer, 7: 763-781 (1964).

18. Langhaar, H. L. "Steady Flow in the Transition Length for a Straight Tube," Journal of Applied Mechanics, 64: A55-A58 (1942).

19. Shah, R. K. "Laminar Flow Friction and Forced Convection Heat Transfer in Ducts of Arbitrary Geometry," Int. Journal of Heat and Mass Transfer, 18: 849-862 (1975).

20. Binder. Fluid Mechanics (Fourth Edition). New York: Prentice Hall, Inc., 1962.

21. Wiginton, C. L. and C. Dalton. "Laminar Flow in the Entrance Region of a Rectangular Duct," Journal of Applied Mechanics, 37: 854-856 (1970).

22. Fleming, D. P. and E. M. Sparrow. "Flow in the Hydrodynamic Entrance Region of Ducts of Arbitrary Cross Section," Journal of Heat Transfer, 91: 345-354 (1969).

23. Han, L. S. "Hydrodynamic Entrance Lengths for Incompressible Laminar Flow in Rectangular ducts," Journal of Applied Mechanics, 27: 403-409 (1960).

24. McComas, S. T. "Hydrodynamic Entrance Lengths for Ducts of Arbitrary Cross Section," Journal of Basic Engineering, 89: 847-850 (1967).

25. Manohar, R. "An Exact Analysis of Laminar Flow in the Entrance Region of an Annular Pipe," Z.Angew. Math. Mech., 45: 171-176 (1965).

26. Roy, D. N. "Laminar Flow Near the Entry of Coaxial Tubes," Applied Science Research, 14: 421-430 (1965).

27. Coney, J. E. R. and M. A. I. El-Shaarawi. "Developing Laminar Radial Velocity Profiles and Pressure Drop in the Entrance Region of Concentric Annuli, <u>Nuclear Science Engineering</u>, <u>57</u>: 169-174 (1975).

28. Sparrow, E. M. and S. H. Lin. "The Developing Laminar Flow and Pressure Drop in the Entrance Region of Annular Ducts," <u>Journal of Basic Engineering</u>, <u>86</u>: 827-834 (1964).

29. Ghiglieri, Lt J. C. Correspondence. APFL Wright-Patterson AFB OH. 29 Jan 1965.

VITA

Captain Bruce J. Sutherland was born on 20 July 1959 in Memphis, Tennessee. He graduated from Frank W. Cox High School in 1977 and attended the United States Air Force Academy from which he received the degree of Bachelor of Science in Aeronautical Engineering in June 1982. Upon graduation, he received a commission in the USAF, and was employed by Aeronautical Systems Division, Aerodynamics and Performance Branch, Wright-Patterson AFB, Ohio, until entering the School of Engineering, Air Force Institute of Technology, in July 1985.

Permanent address: 225 S. W. 8th Circle
Cedaridge, Colo. 81413

REPORT DOCUMENTATION PAGE

1a. REPORT SECURITY CLASSIFICATION UNCLASSIFIED	1b RESTRICTIVE MARKINGS
2a. SECURITY CLASSIFICATION AUTHORITY	3. DISTRIBUTION / AVAILABILITY OF REPORT Approved for public release; distribution unlimited
2b. DECLASSIFICATION / DOWNGRADING SCHEDULE	

4. PERFORMING ORGANIZATION REPORT NUMBER(S) AFIT/GAE/AA/86D-17	5 MONITORING ORGANIZATION REPORT NUMBER(S)

6a. NAME OF PERFORMING ORGANIZATION School of Engineering	6b OFFICE SYMBOL (If applicable) AFIT/ENY	7a. NAME OF MONITORING ORGANIZATION

6c. ADDRESS (City, State, and ZIP Code) Air Force Institute of Technology Wright-Patterson AFB, OH 45433	7b. ADDRESS (City, State, and ZIP Code)

8a. NAME OF FUNDING / SPONSORING ORGANIZATION	8b OFFICE SYMBOL (If applicable)	9 PROCUREMENT INSTRUMENT IDENTIFICATION NUMBER

8c. ADDRESS (City, State, and ZIP Code)

10 SOURCE OF FUNDING NUMBERS

PROGRAM ELEMENT NO.	PROJECT NO.	TASK NO	WORK UNIT ACCESSION NO

11. TITLE (Include Security Classification)

A Redefined Hydraulic Diameter For Laminar Flow

12. PERSONAL AUTHOR(S)
Sutherland, Bruce John, B.S., Captain, USAF

13a. TYPE OF REPORT M.S. Thesis-Final Draft	13b. TIME COVERED FROM Jul 85 TO Dec 86	14. DATE OF REPORT (Year, Month, Day) 1986, Dec., 1	15. PAGE COUNT 111

16. SUPPLEMENTARY NOTATION

17. COSATI CODES			18 SUBJECT TERMS (Continue on reverse if necessary and identify by block number)
FIELD	GROUP	SUB-GROUP	Laminar Flow, Hydraulic Diameter, Transition Reynolds Number; Hydrodynamic Entrance Length

19. ABSTRACT (Continue on reverse if necessary and identify by block number)

Title: A Redefined Hydraulic Diameter For Laminar Flow

Thesis Chairman: Dr. James Hitchcock

Cont. on reverse

20. DISTRIBUTION / AVAILABILITY OF ABSTRACT ☒ UNCLASSIFIED/UNLIMITED ☐ SAME AS RPT ☐ DTIC USERS	21 ABSTRACT SECURITY CLASSIFICATION UNCLASSIFIED
22a. NAME OF RESPONSIBLE INDIVIDUAL Dr. James Hitchcock	22b TELEPHONE (Include Area Code) (513) 255-3517	22c OFFICE SYMBOL AFIT/ENY

DD Form 1473, JUN 86   Previous editions are obsolete   SECURITY CLASSIFICATION OF THIS PAGE

Abstract

For laminar, steady flow in ducts, the current definition of hydraulic diameter, D_h, does not accurately depict the non-uniform wall shear stress distribution around the perimeter of non-circular duct shapes. In this investigation, a new hydraulic diameter, $D_{h,l}$, was empirically determined. It correlated friction factor data for many non-circular shapes to within approximately 2.4 % of the circular duct value.

An experiment, using the AFIT Oil Flow Rig Set-up, was run to determine the effect on transition Reynolds number, Re_{tr}, and hydrodynamic entrance length, L^*, of replacing D_h with $D_{h,l}$. Transition Reynolds number and L^* were determined, based on D_h and $D_{h,l}$, for a circular, square, and concentric annular duct.

Transition Reynolds numbers, based on D_h, for the square and concentric annular ducts were approximately 12.5 % lower than the circular duct Re_{tr}. The Re_{tr}, based on $D_{h,l}$, did not correlate well for the concentric annulus, but did correlate for the square duct.

Hydrodynamic entrance lengths, based on D_h and $D_{h,l}$, were experimentally determined for the circular and square duct only. The square duct L^*, and the analytic concentric annular duct L^*, based on $D_{h,l}$, did not correlate to the circular duct value.

Although the Re_{tr} and L^* for the square and concentric annular ducts did not correlate well when based on $D_{h,l}$, the data obtained is still useful to the engineering community since it provides an addition data base for experimental L^*, and provides experimental data on Re_{tr} for square and concentric annular ducts.

END

5-87

DTIC